An efficient method of moments for simulating atmospheric aerosol growth: model description, verification and application

J. Shen[1], Y. Liu[1], C. Tu[1], M. Yu[2*], T.L. Chan[3]

[1] China Jiliang University, Hangzhou, China

[2] Department of Atmospheric Science, Zhejiang University, Hangzhou, China

[3] Department of Mechanical Engineering, The Hong Kong Polytechnic University, Kowloon, Hong Kong

Corresponding author: M. Yu (yumz@ieecas.cn)

Key Points:

- Atmospheric aerosol dynamics model
- Method of moments
- Hybridization
- Taylor-series expansion method of moments
- Method of moments with log-normal size distribution

Abstract

The atmospheric aerosol dynamics model (AADM) has been widely used in both comprehensive air quality model systems and chemical transport modeling from road to global scales. The AADM consists of the Smoluchowski coagulation equation (SCE) which describes the atmospheric aerosol size growth due to coagulation. The numerical solution to the SCE undergoing Brownian coagulation in the free molecular regime is a direct challenge because of a stumbling block for the kernel to be expressed by an equivalent linear expression and a predefined lognormal size distribution, which is inconsistent with aerosols having bimodal or multimodal size distribution. Thus, a new mathematical method for solving the SCE without the strong assumption of log-normal size distribution is proposed and developed. This method is verified with a referenced sectional method (SM) with excellent agreement. The accuracy of the method approaches closely to the TEMOM, but overcomes the limitation of the classical log MOM. The computational time of this scheme is largely reduced when comparing to the SM. The new method is successfully implemented to reveal the formation and growth of secondary particles emitted from the vehicle exhaust tailpipe. It is surprisingly found that the formation of new particles only appears in the interface region of the turbulent exhaust jet which is very close to the tailpipe exit, while there is no new particle formation in the strong mixture along the downstream. The new method is finally verified to be an efficient and reliable numerical scheme for studying atmospheric aerosol dynamics.

1 Introduction

There has been increased recognition of the importance of aerosols to both climate change (Rosenfeld, 2006; Rosenfeld et al., 2014, 2019) and air pollution (Huang et al., 2014; Kumar et al., 2014; Y. Wang et al., 2019; Yao et al., 2018; Yuan et al., 2019). Correspondingly, the inclusion of the aerosol dynamics models in both global chemistry and transport simulations and regional air quality simulations has been carried out over half a century (Gama et al., 2019; Hass et al., 2003; Herzog et al., 2004; Jasor et al., 2005; Karydis et al., 2007; Lauer et al., 2005; Sportisse, 2007; Vignati et al., 2004; Whitby & McMurry, 1997; C. Zhou et al., 2016). In all developed aerosol dynamics models, aerosol dynamics which dominates the evolution of particle size distribution are dealt with separately to meet the requirement of numerical simulation. These aerosol dynamic processes usually include nucleation, coagulation, condensation-evaporation, deposition, etc. Brownian coagulation is an important mechanism leading to the instability of aerosols, which is also attracted more interest by scientists than other aerosol dynamics because it is not easily dealt with mathematically. The end result of coagulation is a continuous decrease in particle number concentration and an increase in particle size. The theory for illustrating this phenomenon was originally introduced from Smoluchowski's equation and was then followed by Muller's development (Müller, 1928; Petitti et al., 2013). The Muller's equation is expressed as,

$$\frac{\partial n(v,t)}{\partial t} = \frac{1}{2}\int_0^v \beta(v_1, v-v_1)n(v_1,t)n(v-v_1,t)\mathrm{d}v_1 - n(v,t)\int_0^\infty \beta(v_1,v)n(v_1,t)\mathrm{d}v_1 \quad (1)$$

where particle volume, v, is used rather than particle diameter because the volumes are additive. The first term on the right-hand side of Equation (1) is the rate of formation of particles of size v by smaller particles of sizes v_1 and $v - v_1$. The factor $1/2$ is introduced because collisions are counted twice in the integral. The second term of Equation (1) accounts for the loss of particles of size v by collisions with all other particles. Equation (1) was known as Smoluchowski's Coagulation Equation (SCE), which was further developed later in the community of aerosols to include other aerosol dynamic processes including nucleation, condensation-evaporation, deposition and also to couple with climate models by considering air convection and diffusion. The developed Equation (1) is recognized now as the particle general dynamics equation (PGDE), which is the key equation of all weather and air pollution forecast codes, including Weather Research and Forecasting model coupled to Chemistry (WRF-Chem), University of Helsinki Multicomponent Aerosol model and European Air Pollution Dispersion modelling system (EURAD (Ackermann et al., 1998; Grabowski et al., 2019; Korhonen et al., 2004; Kukkonen et al., 2012).

In theory, almost all important aerosol quantities, which determine the property of aerosol as well as it directly or indirectly affects air pollution and

climates, such as number concentration, mass concentration and size distribution of particles, can be obtained by solving the PGDE numerically(Wright et al., 2001). The PGDE is usually solved by numerical methods and there have been some important achievements including the sectional method (SM) (Bruns & Ezekoye, 2012; Gelbard et al., 1980; Kostoglou, 2007; Landgrebe & Pratsinis, 1990), method of moments (MOM) (Fox et al., 2008; S. Liu, Chan, Lin, et al., 2019; Petitti et al., 2013; Pratsinis, 1988; Rani et al., 2014; Tang & Lin, 2013), Monte Carlo (MC) method (Kraft, 2005; Morgan et al., 2006), and stochastic particle method (Debry et al., 2003; Kruis et al., 2012; Menz et al., 2014; Rani et al., 2014; Sabelfeld, 1998). Now, these three different types of numerical methods have been widely applied in weather and air pollution forecast codes. Among all these three numerical methods, the MOM is usually regarded as the most economic one and is also the most suitable to be coupled with the air transport equation, such as Navier-Stokes equations (McGraw et al., 2008; Passalacqua et al., 2018; Yu & Lin, 2018) To be noted here, the MOM with predefined log-normal size distribution is still the classical method used in the most common weather and air pollution forecast codes, such as WRF-Chem and EURAD (Cai et al., 2016; Gama et al., 2019). It should be noted that the SM is also used for modeling aerosol dynamics in nuclear reactor safety (Herranz et al., 2018).

The key of the MOM is to implement a transformation from particle size distribution (PSD) function space, $\{n(v)\}$ in Equation (1), to the space of moments, $\{m_k\}$. When transferring from $\{n(v)\}$to $\{m_k\}$, the closure problem for ordinary differential equations (ODEs) appears which needs to be resolved using closure schemes. There have been several schemes to achieve closure, which can be divided into two categories, namely quadrature-based MOM (QBMOM) and non-quadrature-based MOM (NBMOM). The predefined particle size distributed method, pth-order-polynomial MOM, MOM with interpolative closure (MOMIC) and Taylor series expansion MOM belong to the NBMOM. An advantage of the NBMOM is that the transferred moment ODEs can be written as its explicit form (Yu & Lin, 2018). It should be noted that the QBMOM, especially Gaussian quadrature MOM (QMOM and direct QMOM (DQMOM)) (Marchisio & Fox, 2005; Robert McGraw, 1997a) is the most widely used MOM to couple with computational fluid dynamics (CFD) until nowadays. Among all the NBMOMs, the predefined log-normal MOM was the first proposed for solving PGDE (Cohen & Vaughan, 1971), and now it governs the establishment of atmospheric aerosol models, including WRF-Chem and EURAD. When implementing the log-normal MOM by transferring from the particle size distribution function space, $\{n(v)\}$ to the space of moments, $\{m_k\}$, the collision kernel must be written as an equivalent linear expression for $v^p v_1^q$ (p and q are arbitrary real numbers). This requirement limits the application of log MOM because some kernels cannot easily be obtained with an equivalent linear expression for $v^p v_1^q$. Although the QBMOM is the widely used MOMs today due to main contributions from the research groups of Fox (Heylmun et al., 2019; Kong & Fox, 2017; Marchisio & Fox, 2005; Vikas et al., 2013) and McGraw (McGraw et al., 2008; McGraw, 1997b), the NBMOM, such as the log MOM and TEMOM, can still find its

wide applications due to their high numerical efficiency without eigensystems' calculation and ill-conditioned matric problems.

Brownian coagulation in the free molecular is a key mechanism affecting the evolution of aerosol size distribution with particle Knudsen number (Kn = $\frac{\lambda}{r}$, where λ is the mean free path of air, and r is particle diameter) larger than 50 (Park et al., 1999a). The collision kernel in this regime has a term $(1/v + 1/v_1)^{1/2}$, which is the major stumbling block for the kernel to be expressed by an equivalent linear expression, so does the transfer of SCE to the moment ODEs. Some efforts have been made to overcome this technical difficulty. The most success is the strategy proposed by Lee et al. (1984), in which the factor $(1/v + 1/v_1)^{1/2}$ was substituted by $b[(1/v)^{1/2} + (1/v_1)^{1/2}]$; the SCE can then be transferred to moment ODEs with both implicit and explicit moments. In order to achieve the final closure of moment ODEs, Equation (11) below is needed. Unfortunately, the value of b is an unmanageable issue in Equation (9) below, which has to be obtained through solving integral equations with varying initial particle size distributions. Pratsinis (1988) then further developed and expressed the term, b , as a function of geometric standard deviation of particle size distribution. However, both of their studies have the limitation that the expression of the value b has to be determined numerically in advance, which inevitably leads to uncertain in mathematics. Hence, a high efficient and precise method becomes essential to approximate this collision kernel.

The TEMOM was proposed by Yu et al. (2008) to solve SCE. The key of the TEMOM is to approximate any expressions using their truncated Taylor expansion series with adjusted errors, thus the technical difficulty in the log MOM might be overcome by the TEMOM. Although the TEMOM has been successfully applied to solve the SCE due to Brownian coagulation in the free molecular regime, $(1/v + 1/v_1)^{1/2}$ and implicit moments are both implemented by the Taylor-series expansion technique. Whether $(1/v + 1/v_1)^{1/2}$ is implemented by the TEMOM and implicit moments are implemented by the log MOM simultaneously or conversely, it remains an open question.

In the present study, a new method to explicitly solve the SCE undergoing Brownian coagulation in the free molecular regime is presented. The underlying idea of this method is that the approximations of collision kernel and explicit moments are achieved by the hybridization of the well-established log MOM and TEMOM. For distinguishing this new hybrid method from other MOMs, a hybrid TEMOM-log MOM is used. Since there are two different hybrid processes involvement, namely hybrid TEMOM-log MOM (I) and hybrid TEMOM-log MOM (II), are used for their distinguishment. The SM as a reference is used to validate this new scheme of hybrid TEMOM-log MOM, which has regarded as an exact solution of SCE by the aerosol society (Otto et al., 1999) as well as our previous works (Yu et al., 2016; Yu & Lin, 2017a). In addition, the results from both TEMOM and log MOM are presented for comparative studies. The moment ODEs obtained from the proposed scheme have the explicit expressions, thus to be easier programed than the well-established log MOM.

The newly proposed hybrid TEMOM-log MOM (I) is further utilized to study the formation and growth of secondary particles emitted from the vehicle exhaust tailpipe, in which an advanced parameterized model for binary homogeneous nucleation of sulfuric acid-water vapors is introduced. The competing processes of binary nucleation, condensation and coagulation are clearly revealed.

The paper is organized as follows: In Section 2, the model description related to the hybrid TEMOM-log MOM method is presented, and the numerical errors are fully analyzed. In Section 3, the numerical details of studied cases are provided and all the governing equations are dealt with a normalized method. In Section 4, the results and discussion are presented for the comparison among new hybrid TEMOM-log MOM, TEMOM, log MOM, and SM, and the validation of the new method is carried out. In this section, the new scheme is further utilized to study the exhaust particles emitted from the vehicle tailpipe. The factors affecting the secondary nanoparticle formation and subsequent growth in a turbulent jet exhaust plume are revealed.

2 Materials and Methods

In the present study, Brownian coagulation in the free molecular regime is considered because it is the most difficult to deal with using the MOM (Pratsinis,1988). For the studied case, the coagulation kernel is given by (Friedlander, 2000):

$$\beta(v, v_1) = B_1(1/v + 1/v_1)^{1/2}(v^{1/3} + {v_1}^{1/3})^2 \qquad (2)$$

where $B_1 = (3 / 4\pi)^{1/6}\left(6k_{\mathrm{B}}T / \rho_{\mathrm{p}}\right)^{1/2}$, k_{B} is the Boltzmann constant, T is the gas temperature and ρ_{p} is the mass density of the particles.

In order to implement the MOM, the system of Equation (1) is transferred to a system of moment ODEs with respect to the moment. The moment transformation involves multiplying Equation (1) by v and then integrating over the entire particle size distribution, and then the moment transformed equations of the PSD are obtained (Lee et al., 1984):

$$\frac{\mathrm{d}m_k}{\mathrm{d}t} = \frac{1}{2}\int_0^\infty \int_0^\infty \kappa(v, v_1, k)n(v, t)n(v_1, t)\mathrm{d}v\mathrm{d}v_1 \qquad (3)$$

where $\kappa(v, v_1, k) = [(v + v_1)^k - v^k - {v_1}^k]\beta(v, v_1)$ and the moment m_k is defined by:

$$m_k = \int_0^\infty v^k n(v)\,\mathrm{d}v \qquad (4)$$

The dynamic behavior of an aerosol can be described from the rate of change of its first three moments(Pratsinis, 1988). According to the present study on the log MOM and TEMOM, only the first three moments are considered here,

$$\kappa(v, v_1, k) = [(v + v_1)^k - v^k - {v_1}^k]\beta(v, v_1)$$

$$= \begin{cases} -\beta(v, v_1), & k = 0, \\ 0, & k = 1, \\ 2vv_1\beta(v, v_1), & k = 2. \end{cases} \quad (5)$$

2.1. Two technical difficulties in the MOM

If only k = 0, 1 and 2 are involved, Equation (3) can be written as

$$\begin{cases} \dfrac{\mathrm{d}m_0}{\mathrm{d}t} = -\dfrac{1}{2}\displaystyle\int_0^\infty \int_0^\infty \beta(v, v_1)n(v, t)n(v_1, t)\mathrm{d}v\mathrm{d}v_1, \\ \dfrac{\mathrm{d}m_1}{\mathrm{d}t} = 0, \\ \dfrac{\mathrm{d}m_2}{\mathrm{d}t} = \displaystyle\int_0^\infty \int_0^\infty vv_1\beta(v, v_1)n(v, t)n(v_1, t)\mathrm{d}v\mathrm{d}v_1. \end{cases} \quad (6)$$

The purpose of the MOM is to remove an integral operator on the right hands of Equation (6). Unfortunately, two essential technical difficulties arise from the particle size distribution function space, $\{n(v)\}$, to the space of moments, $\{m_k\}$, i.e. the binary polynomial approximation and the closure function for any order moment.

2.1.1 Binary polynomial approximation

To introduce the Equation (4) into Equation (6), the collision kernel, $\beta(v, v_1)$ must be expressed as a binary additive form, i.e.,

$$\tilde{\beta}(v, v_1) = \sum_{p\in R}\sum_{q\in R} a_{pq}v^p{v_1}^q \approx \beta(v, v_1) \quad (7)$$

where p and q are arbitrary real numbers, a_{pq} is coefficient. Unfortunately, the presence of the term $(1/v + 1/v_1)^{1/2}$ in Equation (2) makes the binary additive form unavailable.

2.1.2 Closure function

Even if Equation (7) is available and the terms on the right sides of Equation (6) can be expressed as functions of moments, these moments are usually not explicit which makes the non-closure of transferred moment ODEs. A general closure function that can be used to replace any k-th moments becomes necessary. In

Equation (6), only the first three moments, namely m_0, m_1 and m_2, are explicit, and thus the general closure function can be expressed as,

$$m_k = f_{\text{closure}}(m_0, m_1, m_2) \quad (8)$$

where k is an arbitrary real number.

It should be noted that both log MOM and TEMOM have the same above mentioned problems, and the corresponding solutions of them have been given by direct and explicit formulations as Equations (7) and (8).

2.2. Two polynomial approximations to the kernel in the free-molecule regime

2.2.1. log-normal kernel (Log-kernel)

In the previous work of Lee et al (1984), the term $(1/v + 1/v_1)^{1/2}$ is approximated as

$$(\frac{1}{v} + \frac{1}{v_1})^{1/2} \approx b\left(\frac{1}{v^{1/2}} + \frac{1}{v_1^{1/2}}\right) \quad (9)$$

where

$$b = \int_0^\infty \int_0^\infty v^k \beta(v, v_1) n(v, t) n(v_1, t) \mathrm{d}v \mathrm{d}v_1$$

$$\times \{\int_0^\infty \int_0^\infty \left[\frac{\left(\frac{1}{v^{1/2}} + \frac{1}{v_1^{1/2}}\right)}{(v + v_1)^{1/2}}\right] \times v^k \beta(v, v_1) n(v, t) n(v_1, t) \mathrm{d}v \mathrm{d}v_1\}^{-1} \quad (10)$$

To obtain the coefficient b in Equation (10), the numerical calculation must be carried out. In addition, b is a value depending on the initial geometric standard deviation, σ_0 in the work of Lee et al. (1984) and Pratsinis (1988). It implies that b has different values for different particle size distribution. This makes the approach to deal with the uncertainty of $(1/v + 1/v_1)^{1/2}$ in mathematics. Although Pratsinis (1988) tried to write b as a function of σ_0, the relative errors to real values of such an approach cannot be obtained. Furthermore, for calculating the value of b, many hypotheses and simplifications have to be involved, including the assumption of time-dependent log-normal size distribution. It leads to the motivation for developing a more reliable way in order to deal with the approximation of $(1/v + 1/v_1)^{1/2}$ in the present study.

The collision kernel in the free molecular regime, i.e. Equation (2), can be further expressed if the log MOM is implemented as follows,

$$\beta(v,v_1) = Kb_k\left(v^{\frac{2}{3}}v_1^{-\frac{1}{2}} + 2v^{\frac{1}{3}}v_1^{-\frac{1}{6}} + v_1^{\frac{1}{6}} + v^{\frac{1}{6}} + 2v^{-\frac{1}{6}}v_1^{\frac{1}{3}} + v^{-\frac{1}{2}}v_1^{\frac{2}{3}}\right)$$

$$\triangleq \tilde{\beta}_{\mathrm{Log}}(v,v_1) \qquad (11)$$

Here, the approximating kernel $\tilde{\beta}_{\mathrm{Log}}(v,v_1)$ is called a log-normal kernel (Log-kernel).

2.2.2. Binary Taylor expansion kernel (Taylor-kernel)

In the TEMOM, the term $(1/v + 1/v_1)^{1/2}$ is approximated with a binary additive form by implementing a binary Taylor-series expansion technique (Mingzhou Yu et al., 2008). Without loss of generality, $f(v,v_1) = (v+v_1)^{1/2}$ can then be defined as,

$$f(v,v_1) =$$

$$f(u,u) + \left[(v-u)\frac{\partial}{\partial v} + (v_1-u)\frac{\partial}{\partial v_1}\right]f(u,u) +$$

$$\frac{1}{2!}\left[(v-u)\frac{\partial}{\partial v} + (v_1-u)\frac{\partial}{\partial v_1}\right]^2 f(u,u) + \cdots +$$

$$\frac{1}{n!}\left[(v-u)\frac{\partial}{\partial v} + (v_1-u)\frac{\partial}{\partial v_1}\right]^n f(u,u) + \frac{1}{(n+1)!}\left[(v-u)\frac{\partial}{\partial v} + (v_1-u)\frac{\partial}{\partial v_1}\right]^{n+1} f(u+$$

$$\theta(v-u), u+\theta(v_1-u)), (0<\theta<1). \qquad (12)$$

The error R_n is denoted as

$$R_n = \frac{1}{(n+1)!}\left[(v-u)\frac{\partial}{\partial v} + (v_1-u)\frac{\partial}{\partial v_1}\right]^{n+1} f(u+\theta(v-u), u+\theta(v_1-u)), \qquad (13)$$

and the absolute error$|R_n|$ is denoted as

$$|R_n| \le \frac{M}{(n+1)!}(|v-u| + |v_1-u|)^{n+1} = \frac{M}{(n+1)!}\rho^{n+1}(|\cos\alpha| + |\sin\beta|)^{n+1}$$

$$= \frac{(\sqrt{2})^{n+1}}{(n+1)!}M\rho^{n+1} \qquad (14)$$

where M is a positive number and $\rho = \sqrt{(v-u)^2 + (v_1-u)^2}$. When $\rho \to 0$, i.e., $v \to u$ and $v_1 \to u$ simultaneously, the absolute error $|R_n| \to 0$ and the rate of convergence is $O(\rho^{n+1})$. It implies the binary additive form in Equation (12) is theoretically reasonable when the volume of aerosol particles approaches the average

value. If the Taylor-series expansion point is u, the term $(1/v + 1/v_1)^{1/2}$ is approximated by the following expression,

$$(v+v_1)^{1/2} \approx \frac{3\sqrt{2u}}{8} + \frac{3\sqrt{2}v}{8\sqrt{u}} + \frac{3\sqrt{2}v_1}{8\sqrt{u}} - \frac{\sqrt{2}v^2}{32u^{3/2}} - \frac{\sqrt{2}vv_1}{16u^{3/2}} - \frac{\sqrt{2}{v_1}^2}{32u^{3/2}}. \quad (15)$$

Then the collision kernel in the free-molecule regime is now approximated as follows:

$$\begin{aligned}
&\beta(v,v_1) \\
&\approx B_1\left[\frac{3}{8}(2u)^{\frac{1}{2}}(2v^{\frac{1}{6}}v_1^{-\frac{1}{2}} + 2v^{-\frac{1}{6}}v_1^{\frac{1}{6}}) + \frac{3}{8}(\frac{2}{u})^{\frac{1}{2}}(2v^{\frac{7}{6}}v_1^{-\frac{1}{2}} + 4v^{\frac{5}{6}}v_1^{-\frac{1}{6}} + 2v^{\frac{1}{2}}v_1^{\frac{1}{6}})\right. \\
&\left. - \frac{1}{32}(\frac{2}{u^3})^{\frac{1}{2}}(4v^{\frac{5}{6}}v_1^{\frac{5}{6}} + 4v^{\frac{7}{6}}v_1^{\frac{1}{2}} + 2v^{\frac{3}{2}}v_1^{\frac{1}{6}} + 2v^{\frac{13}{6}}v_1^{-\frac{1}{2}} + 4v^{\frac{11}{6}}v_1^{-\frac{1}{6}})\right] \\
&\triangleq \tilde{\beta}_{\text{Taylor}}(v,v_1). \quad (16)
\end{aligned}$$

Here, the approximating kernel $\tilde{\beta}_{\text{Taylor}}(v,v_1)$ is called binary Taylor expansion kernel (Taylor-kernel).

Substituting the log-kernel into Equation (11) and the Taylor-kernel in Equation (16) into the moment ODEs of Equation (5) results in the following system, respectively,

$$\begin{cases} \dfrac{\mathrm{d}m_0}{\mathrm{d}t} = -\dfrac{1}{2}\displaystyle\int_0^\infty\int_0^\infty \tilde{\beta}_{\text{Log}}(v,v_1)n(v,t)n(v_1,t)\mathrm{d}v\mathrm{d}v_1 \\ \dfrac{\mathrm{d}m_1}{\mathrm{d}t} = 0 \\ \dfrac{\mathrm{d}m_2}{\mathrm{d}t} = \displaystyle\int_0^\infty\int_0^\infty vv_1\tilde{\beta}_{\text{Log}}(v,v_1)n(v,t)n(v_1,t)\mathrm{d}v\mathrm{d}v_1. \end{cases} \quad (17)$$

and

$$\begin{cases} \dfrac{\mathrm{d}m_0}{\mathrm{d}t} = -\dfrac{1}{2}\displaystyle\int_0^\infty\int_0^\infty \tilde{\beta}_{\text{Taylor}}(v,v_1)n(v,t)n(v_1,t)\mathrm{d}v\mathrm{d}v_1 \\ \dfrac{\mathrm{d}m_1}{\mathrm{d}t} = 0 \\ \dfrac{\mathrm{d}m_2}{\mathrm{d}t} = \displaystyle\int_0^\infty\int_0^\infty vv_1\tilde{\beta}_{\text{Taylor}}(v,v_1)n(v,t)n(v_1,t)\mathrm{d}v\mathrm{d}v_1. \end{cases} \quad (18)$$

2.3. Two closure functions in the MOM

Both log MOM and TEMOM have been widely verified to be promising methods for solving SCE with very little computational costs. As discussed in Section 2.1, both Equations. (17) and (18) are needed to be further closed using suitable closure functions. In the log MOM, the closure function is obtained based on an assumption of time-dependent log-normal size distribution, whereas in the TEMOM the closure function is obtained by expanding v^k within a manageable error. If the log MOM closure function (Lee et al., 1984) is applied to Equation (17) and the TEMOM closure function (Yu et al., 2008) is applied to Equation (18), the new schemes are presented as below.

2.3.1. Hybrid TEMOM-log MOM (I)

In the TEMOM, the closure function has the following expression,

$$m_k = \left(\frac{u^{k-2}k^2}{2} - \frac{u^{k-2}k}{2}\right)m_2 + \left(-u^{k-1}k^2 + 2u^{k-1}k\right)m_1 + \left(u^k + \frac{u^k k^2}{2} - \frac{3u^k k}{2}\right)m_0 \triangleq m_{k\_\mathrm{Taylor}}, \left(u = \frac{m_1}{m_0}\right) \quad (19)$$

As Equation (19) is applied to Equation (17), a new scheme of hybrid TEMOM-log MOM (I) is derived,

$$\begin{cases} \frac{dm_0}{dt} = B_1 b \frac{m_0^{11/6}\left(41m_0^2m_2^2 - 190m_0m_1^2m_2 - 2443m_1^4\right)}{648m_1^{23/6}} \\ \frac{dm_1}{dt} = 0 \\ \frac{dm_2}{dt} = -B_1 b \frac{65m_0^2m_2^2 - 670m_0m_1^2m_2 - 1987m_1^4}{324m_0^{\frac{1}{6}}m_2^{\frac{11}{6}}}. \end{cases} \quad (20)$$

2.3.2. Hybrid TEMOM-log MOM (II)

In the log MOM, the closure function is obtained by assuming the log-normal particle size distribution (Lee et al., 1984),

$$m_k = m_0^{1-\frac{3}{2}k+\frac{1}{2}k^2} m_1^{2k-k^2} m_2^{-\frac{1}{2}k+\frac{1}{2}k^2}. \quad (21)$$

The derivation of Equation (21) is shown in Appendix 7.3. As Equation (21) is applied to Equation (18), another new scheme of hybrid TEMOM-log MOM (II) for solving SCE can be expressed as

$$\begin{cases} \dfrac{dm_0}{dt} = -\dfrac{B_1}{2}\dfrac{\sqrt{2}m_0^{\frac{59}{36}}}{16m_1^{\frac{29}{9}}m_2^{\frac{7}{36}}}\left(\begin{array}{c} -m_0^{\frac{11}{6}}m_1^{\frac{1}{9}}m_2^{\frac{11}{6}} + 12m_0^{\frac{2}{3}}m_1^{\frac{22}{9}}m_2^{\frac{2}{3}} + 11m_0^{\frac{1}{2}}m_1^{\frac{25}{9}}m_2^{\frac{1}{2}} + 12m_0^{\frac{7}{18}}m_1^{3}m_2^{\frac{7}{18}} \\ +24m_0^{\frac{2}{9}}m_1^{\frac{10}{3}}m_2^{\frac{2}{9}} - 2m_0^{\frac{1}{6}}m_1^{\frac{31}{9}}m_2^{\frac{1}{6}} - 2m_0^{\frac{19}{18}}m_1^{\frac{5}{3}}m_2^{\frac{19}{18}} - 2m_0^{\frac{1}{18}}m_1^{\frac{11}{3}}m_2^{\frac{1}{18}} + 12m_1^{\frac{34}{9}} \end{array}\right) \\ \dfrac{dm_1}{dt} = 0 \\ \dfrac{dm_2}{dt} = -\dfrac{B_1}{2}\dfrac{\sqrt{2}m_0^{-\frac{25}{36}}}{8m_1^{\frac{41}{9}}m_2^{\frac{5}{36}}}\left(\begin{array}{c} m_0^{\frac{23}{6}}m_1^{\frac{1}{9}}m_2^{\frac{31}{9}} - 24m_0^{\frac{11}{9}}m_1^{\frac{16}{3}}m_2^{\frac{5}{6}} - 12m_0^{\frac{5}{3}}m_1^{\frac{40}{9}}m_2^{\frac{23}{18}} + 2m_0^{\frac{13}{6}}m_1^{\frac{31}{9}}m_2^{\frac{16}{9}} + 2m_0^{\frac{55}{18}}m_1^{\frac{5}{3}}m_2^{\frac{8}{3}} \\ +2m_0^{\frac{37}{18}}m_1^{\frac{11}{3}}m_2^{\frac{5}{3}} + m_0^{\frac{5}{2}}m_1^{\frac{25}{9}}m_2^{\frac{19}{9}} - 12m_0^{\frac{1}{2}}m_1^{\frac{61}{9}}m_2^{\frac{1}{9}} - 12m_0m_1^{\frac{52}{9}}m_2^{\frac{11}{18}} - 12m_0^{\frac{7}{18}}m_1^{7} \end{array}\right) \end{cases} \tag{22}$$

2.4. Family of TEMOM-log MOM

According to the above-mentioned schemes, four MOM models can be classified for solving SCE through adjusting the combination of the binary polynomial kernels and the closure functions, which constitutes a family of TEMOM-log MOM

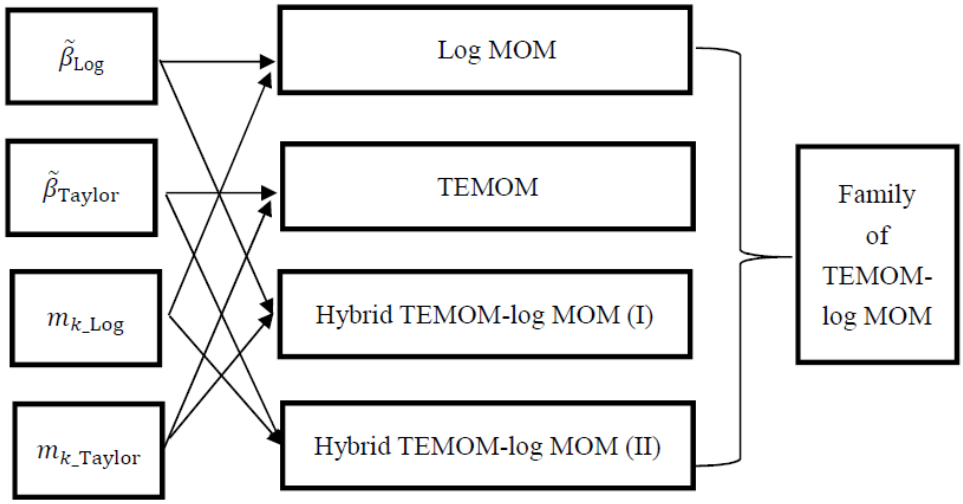

Figure 1 Spanning map of the family of TEMOM-log MOM.

Both the log MOM and TEMOM have been verified as reliable methods for solving SCE. However, the newly proposed and developed hybrid TEMOM-log MOM (I) and (II) have never been verified before. Equations (20) and (22) have explicit expressions, thus the numerical algorithms can be written using a very simple way. In the well-established log MOM widely used in AADM (Pratsinis, 1988), however, the ODEs have to be closed using a log-normal size distributed assumption.

3 Computational description

The SM is selected as a reference and is implemented under the same condition as the hybrid TEMOM-log MOM (I) and (II) models. The relative errors of the hybrid

TEMOM-log MOM (I) and (II) models to the SM are discussed in Section 4. In the present study, the SM model is usually used for validating MOMs which is solved using the same computer code as that used in (Yu & Lin, 2017b). The log MOM and TEMOM are also implemented for comparison purposes. The solution with the assumption of an initial log-normal particle size distribution is used (Barrett & Jheeta, 1996). Hence, k-th moment can be represented by

$$m_k = M_k\left(N_0 v_{g_0}^k\right) \quad (23)$$

where v_{g_0} is the initial geometric mean volume. When the normalized terms are implemented in the moment ODEs as shown in Equations (20) and (23), N_0 and v_{g_0} are included in the normalized time. Under this condition, the dimensionless time with respect to the coagulation kernel in the free molecular regime is

$$\tau = B_1 N_0 v_{g_0}^{1/6} t \quad (24)$$

When the Equation (25) is introduced into Equations (20) and (22), the normalized equations for the hybrid models (I) and (II) are obtained, which are presented in Appendix 7.4. The initial moments can be expressed as

$$M_{k0} = \chi^{k^2} \quad (25)$$

where $\chi = e^{(3\ln\sigma_{g0})^2/2}$. The normalization using Equations (23-25) are applied to the study in Sections 4.1 and 4.3. To be consistent with the study in Yu et al. (2009)., $N_0 = 5.0 \times 10^{19}$ #/m^3 and $d_{g0} = 0.4 \times 10^{-9}$ m . d_{g0} is selected for the diameter of the H_2SO_4 molecular.

4 Results and Discussion

Both the numerical precision and efficiency of the newly proposed method for solving SCE are evaluated to verify its reliability in Sections 4.1 and 4.2. In Section 4.3, the application of the newly proposed method in the study of the formation and growth of secondary particles in the turbulent exhaust jet plume is discussed.

4.1 Model validation

The purpose is to verify the numerical precision of the newly proposed and developed hybrid (I) and (II) models. To achieve this, the hybrid models (I) and (II),

log MOM, TEMOM and SM are applied to solve the same SCE under the same conditions. Four crucial moments, namely M_0, $M_{1/3}$, $M_{2/3}$, and M_{2}, are evaluated.

The relative errors of the k-th moments of the investigated methods of moments to the SM are expressed as:

$$\mathrm{RE}\ (\%) = \frac{M_k(\mathrm{MOM}) - M_k(\mathrm{SM})}{M_k(\mathrm{SM})} \qquad (26)$$

where $M_k(\mathrm{MOM})$ is the k-th moments obtained from the investigated method of moments and $M_k(\mathrm{SM})$ is the corresponding moments obtained from the referenced SM. All numerical calculations are implemented using the fourth-order Runge–Kutta method with a fixed time step of 0.001. The SM, log MOM and TEMOM are verified in Park et al. (1999b), Yu et al. (2008; 2015) and Yu & Lin (2017b).

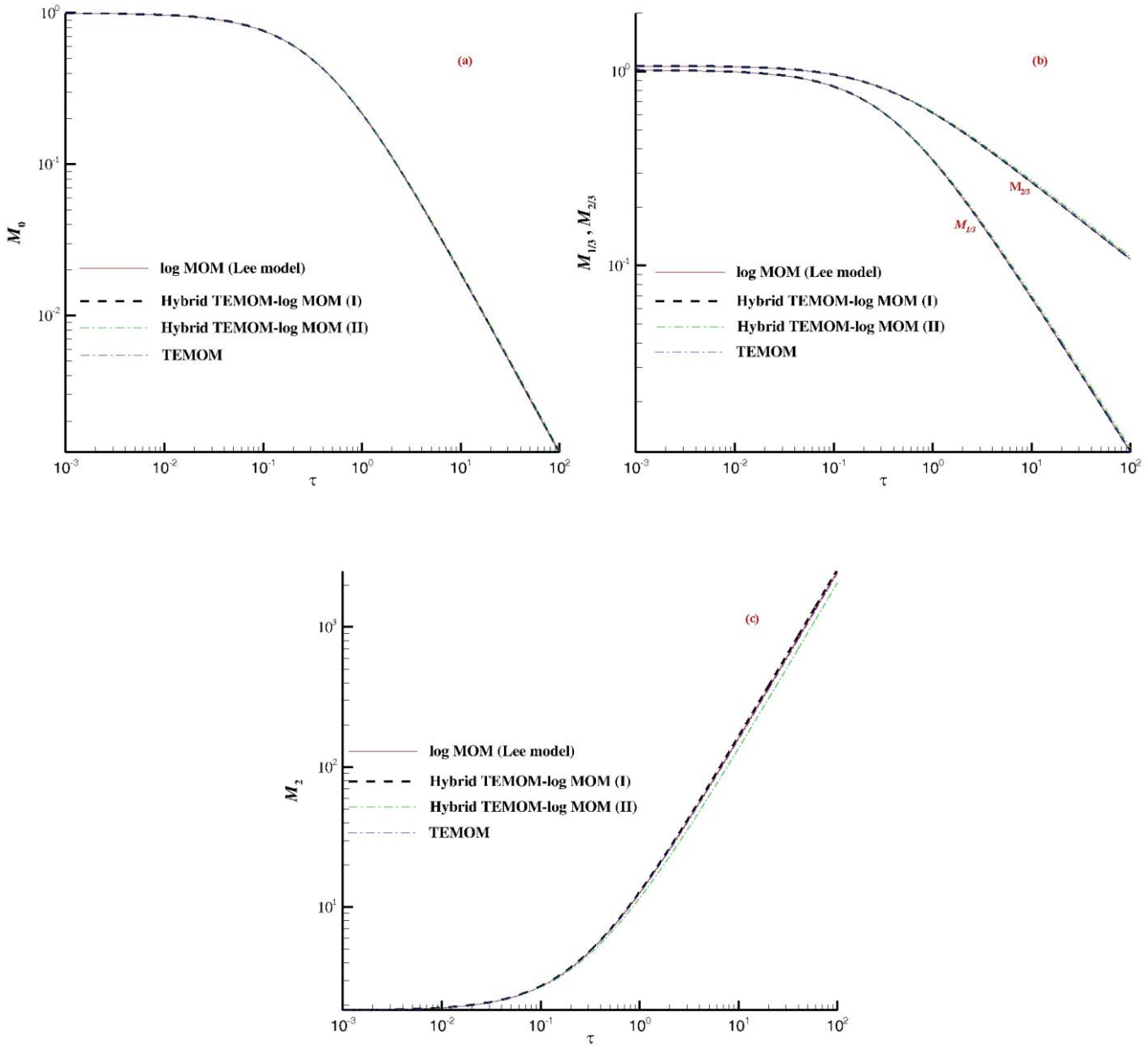

Fig. 2. The variance of *k*-th moments with time produced by the family of TEMOM-log MOM

Fig.2 shows the comparison of the variances of four essential moments with respect to time among these two new hybrid models, log MOM (Lee et al., 1984), and TEMOM (Yu et al., 2008). In the numerical calculation, the initial geometric standard deviation of particle number distribution, $\sigma_{g0} = 1.2$. The zeroth moment, M_0, represents the particle number concentration; the 1/3th moment, $M_{1/3}$, is a quantity characterizing particle surface concentration. The 2/3th moment ($M_{2/3}$) and 2th moment (M_2) have no actual physical meanings, but these two moment variables are essential parts to get other important physical quantities of aerosols such as geometric standard deviation of particle number distribution is given in Equation (27). For three investigated moments, namely M_0, $M_{1/3}$, and $M_{2/3}$, all curves overlap with each other, while for M_2 only the hybrid TEMOM-log MOM (II) deviates slightly from the other three models. The comparison implies that the hybrid TEMOM-log MOM (I), log MOM and TEMOM have nearly the same numerical precision for solving SCE undergoing Brownian coagulation in the free molecular regime. The hybrid TEMOM-log MOM (II) has only a slight difference with the other three models.

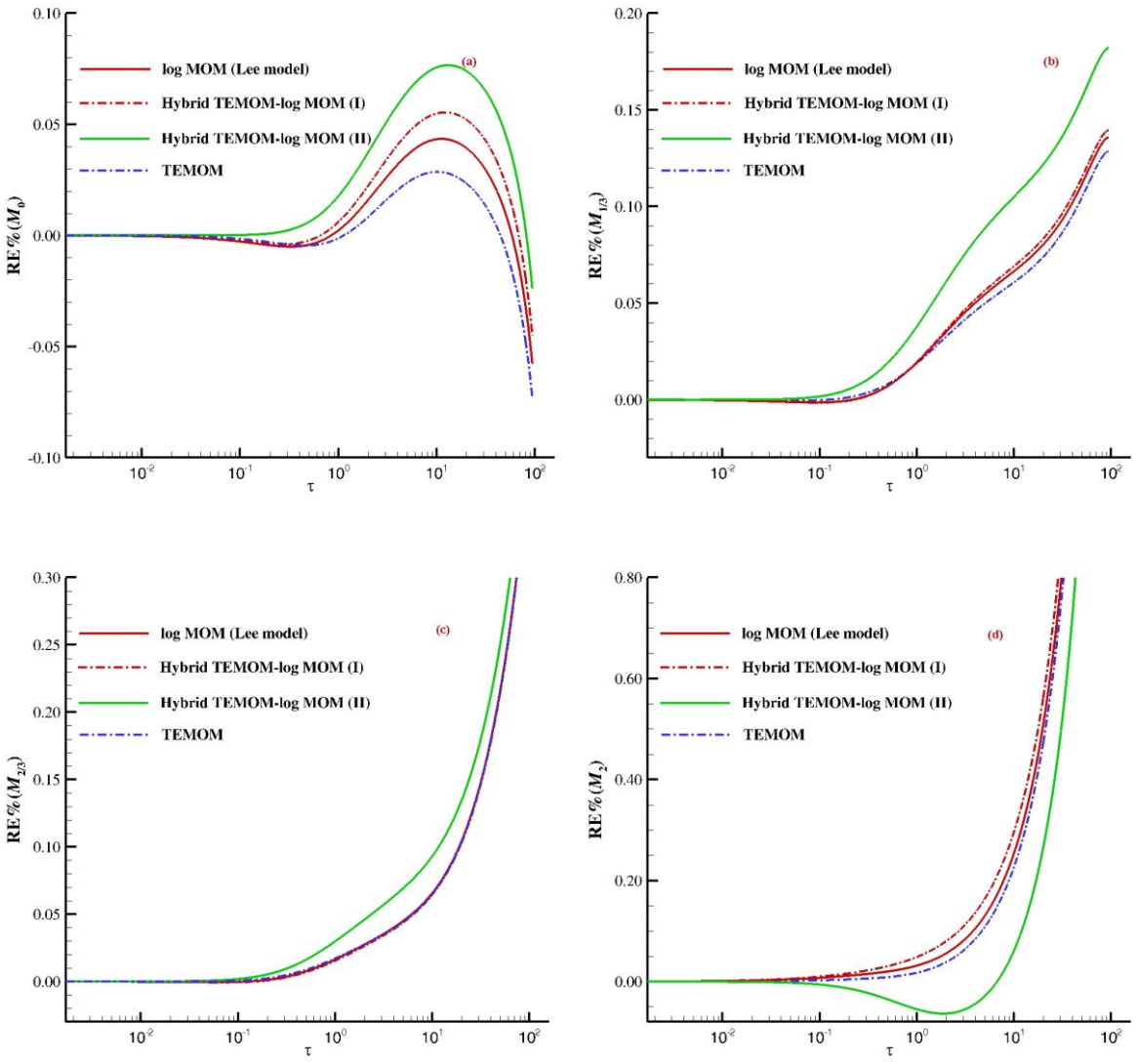

Fig. 3. Relative errors of *k*-th moments of the family of TEMOM-log MOM to the referenced SM in the free molecular regime

For a better evaluation of the reliable new method, the relative errors (REs) of the four moments of the family of TEMOM-log MOM are investigated to the referenced SM as shown in Fig. 3. The SM is usually considered as an exact numerical solution to the SCE (Otto et al., 1999). It is clear that these four methods in the family of TEMOM-log MOM have almost the same variance trend and the maximum relative error of the hybrid TEMOM-log MOM (II) has found in M_0, $M_{1/3}$, $M_{2/3}$, and M_2, respectively. In addition, the other three methods almost overlap with each other especially for $M_{2/3}$. The relative errors of these four methods almost overlap with each other again as $\tau \to 10^2$ for M_0, $M_{2/3}$, and M_2, respectively. It is concluded that the newly proposed and developed hybrid models, especially the TEMOM-log MOM (I) has nearly the same numerical accuracy as the TEMOM and log MOM. As compared with the models of TEMOM-log MOM (I) and (II), the TEMOM-log MOM (I) has higher numerical accuracy.

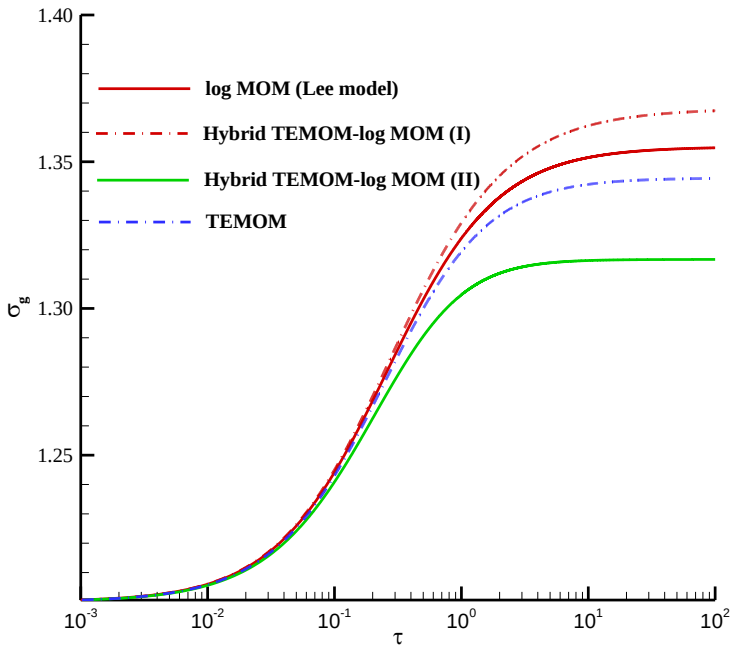

Fig. 4. Comparison of the geometric standard deviations of the particle number distributions derived from the family of TEMOM-log MOM.

The geometric standard deviation, σ_g of the particle number distribution (PSD) is a crucial indicator for characterizing the properties of PSD. The log MOM has the capability to directly produce the value of σ_g according to the first three moments (Lee et al., 1984). The other MOMs such as QMOM and TEMOM are verified to

have the same capability of producing σ_g using the same moments as the log MOM (Yu et al., 2008). Thus, σ_g can be used as an indicator to verify the investigated methods. It is verified that this method has the ability to capture the polydispersity of particle size distribution. If an aerosol can be assumed to be a log-normal particle size distribution, σ_g can be expressed as a function of the first three moments (Pratsinis, 1988),

$$\ln^2 \sigma_g = \frac{1}{9}\ln\left(\frac{M_0 M_2}{M_1^2}\right) \quad (27)$$

In Fig. 4, the values of σ_g for various investigated methods are presented and compared. The values of σ_g from all MOMs of the family of TEMOM-log MOM achieve their own asymptotic values. The asymptotic value of σ_g of TEMOM is 1.345, which is the closest to the value 1.346 produced by the QMOM with 6 nodes (Yu et al., 2008). As expected, both the hybrid TEMOM-log MOM (I) and (II) models achieve their asymptotic values. The values of σ_g of the log MOM, and the hybrid TEMOM-log MOM (I) and (II) models are 1.355, 1.365 and 1.315, respectively (Yu et al., 2008). The hybrid TEMOM-log MOM (I) model generates nearly the same σ_g as the TEMOM and log MOM, whereas the hybrid TEMOM-log MOM (II) model deviates from the other three investigated methods. It is concluded the hybrid TEMOM-log MOM (I) model is a more precise method than the hybrid TEMOM-log MOM (II) by evaluating the four moments and their geometric standard deviations. The TEMOM-log MOM (I) model has very nearly the same numerical precision as the TEMOM and log MOM in numerical precision.

4.2 Numerical efficiency

Table 1 Computational time through executing the fourth-order Runge-Kutta method with a fixed time step, 0.001.

Methods	Computational time
SM	~72.00 hour
TEMOM	~5.05 s
Log MOM	~6.00 s
TEMOM-log MOM (I)	~5.00 s
TEMOM-log MOM (II)	~8.08 s

The numerical precision and efficiency are equally important to determine the feasibility of any numerical models. Here, all the four investigated moment models as well as the SM, are implemented to $\tau = 100$ The numerical efficiency of investigated models is also evaluated by comparing their computational times. For the SM, the section number is 500, which ensures the high numerical accuracy of this SM method.

Table 1 shows the computational time consumed by different investigated models. The ODEs are all solved numerically by executing the fourth-order Runge-Kutta method with a fixed time step, 0.001 under an Intel(R) Core (TM) i7-3820 CPU and Microsoft Visual Studio ~~**2008**~~. The time step, 0.001 is selected because the numerical accuracy under the same time step has been validated in our previous study (Yu et al., 2008). Relative to all the MOMs, the SM consumes relatively very huge computational time. The consumed time of the TEMOM-log MOM (I) model is nearly the same as TEMOM but is smaller than log MOM and TEMOM-log MOM (II) models. By comparing Equations (22) with (22), the mathematical form of the TEMOM-log MOM (II) is much more complex than that of the TEMOM-log MOM (I), thus the former one needs more numerical calculations at each time step. Therefore, it is concluded that the numerical efficiency of the TEMOM-log MOM (I) model has clearly greater than the SM, log MOM and TEMOM-log MOM (II) models, and is even greater than the well-known TEMOM.

In conclusion, the TEMOM-log MOM (I) model is verified to be a promising model for solving SCE in terms of both numerical efficiency and accuracy. In addition, this model has wider applications than the current log MOM because it overcomes the shortcoming of the log MOM with the pre-requirement of assumed log-normal particle size distribution. In the present study, the TEMOM-log MOM (I) model is utilized to study the secondary nanoparticle formation and subsequent growth in a turbulent jet plume in Section 4.3.

4.3 Application of the TEMOM-log MOM (I) model

In the atmospheric environment, it has been realized that most nanoparticles come from a multicomponent route, i.e. binary homogeneous nucleation process of water-sulfuric acid vapors, whereas a complete theoretical understanding of this phenomenon is still a challenge due to it's complicated chemical/physical processes (Chan et al. 2010a and 2010b, Harrison et al., 2018; Liu & Chan, 2016; Maurya et al., 2018; Nagpure et al., 2011; Olin et al., 2019; Zhou & Chan, 2011). Due to the unignorable contribution of gaseous and particulate emissions which are emitted from the power plants and motor vehicles into the atmosphere (Chan, Liu, et al., 2010; Chan, Zhou, et al., 2010; Chan & Ning, 2005; Ning et al., 2005a; Wang et al., 2006; Zhou & Chan, 2011), a lot of attention has been focused on the secondary particles. Most of the particle number emitted by engines is in the nanoparticle range (i.e., d_p <50 nm), especially with the improvement of advanced engine technologies and aftertreatment devices, much higher concentrations of nanoparticles than older

designs are produced nowadays. More and more evidence confirmed that these nanoparticles might have a more negative effect on human health than micrometer and larger particles(Gnach et al., 2015; Harrison et al., 2018). This has raised a question about how to control the emission of nanoparticles before and after the emission conditions. Hence, it is essential to have a better understanding the dynamic processes of nanoparticle formation and subsequent growth in the atmospheric environment.

The evolution of secondary particles in the exhaust is a complicated physical-chemical process, which involves the momentum, heat and mass transfer, binary homogeneous nucleation, Brownian coagulation, Brownian and turbulent diffusions, condensation and thermophoresis (Liu et al., 2019). The appropriate numerical model is coupled the Navier-Stokes equations for flows and the general dynamic equation for particles. The coupling is implemented in a one-way coupling way since nanoparticles have very little effect on the surrounding continuum.

4.3.1 Governing equations

4.3.1.1 Governing equations for fluid flow

Nanoparticles have very small Stokes number in fluid flows to suggest that particles can follow the fluid without disturbing it. In the present study, the Navier-Stokes equations for incompressible flows are:

$$\frac{\partial u_i}{\partial x_i} = 0, \qquad (28(a))$$

$$\frac{\partial u_i}{\partial t} + u_j \frac{\partial u_i}{\partial x_j} = -\frac{1}{\rho}\frac{\partial p}{\partial x_i} + \frac{\partial}{\partial x_j}\left(\nu \frac{\partial u_i}{\partial x_j}\right), \qquad (28(b))$$

$$\frac{\partial \rho h}{\partial t} + \frac{\partial \rho h u_j}{\partial x_j} = \frac{\partial}{\partial x_j}\left(\frac{k_t}{C_p}\frac{\partial h}{\partial x_j}\right), \qquad (28(c))$$

where u_i is the velocity, p is the filtered pressure, h is the specific enthalpy, k_t is the thermal conductivity, $C_p$is the specific heat at constant pressure, the index i, j is taken as 1, 2 and refers to the x and y directions, respectively. The $k-\varepsilon$ turbulent model scheme is utilized to solve Equation (28) regarding the effect of turbulence on the flow.

4.3.1.2 Governing equations for particles

Within the Smoluchowski mean-field theory, the particle number concentration, $n(v,t)$, is represented as a function in terms of particle volume, v, and time, t. Taking into consideration the physical terms of fluid convection, thermophoretic drift, Brownian and turbulent diffusion, Brownian coagulation, condensation and nucleation, the governing equation for $n(v,t)$ can be expressed as:

$$\frac{\partial n(v,t)}{\partial t}+\underbrace{\frac{\partial\left(u_j n(v,t)\right)}{\partial x_j}}_{\text{convection}}+\underbrace{\frac{\partial\left((u_{th})_j n(v,t)\right)}{\partial x_j}}_{\text{thermophoresis}}=\underbrace{\frac{\partial}{\partial x_j}\left(\Gamma\frac{\partial n(v,t)}{\partial x_j}\right)}_{\text{diffusion}}$$
$$+\underbrace{\frac{1}{2}\int_{v*}^{v}\beta(v-v',v')n(v-v',t)n(v',t)dv'-n(v,t)\int_{v*}^{\infty}\beta(v,v')n(v',t)dv'}_{\text{coagulation}}$$
$$+\underbrace{\frac{\partial GN(v,t)}{\partial v}}_{\text{condensation}}+\underbrace{J(v^*)\delta(v-v^*)}_{\text{nucleation}} \qquad (29)$$

where G is the growth rate of nucleus volume due to condensation, Γ is the sum of the turbulent diffusion and Brownian diffusion coefficients ($\Gamma=\Gamma_t+\Gamma_B$), $\beta(v,v')$ is the coagulation kernel between particles of two volumes as shown in Equation (2), J is the nucleation rate, v^* is the volume of a stable sulfuric acid-water (H_2SO_4-H_2O) monomer**,** δ is the Kronecker Delta function and u_{th} is the thermophoretic velocity.

The Equation (29) is usually called the general dynamics equation (GDE), which cannot be directly coupled with Equation (28) for calculation due to its too many degrees relative to the particle volume v. In order to overcome the shortcoming of the GDE, the suitable numerical scheme is to transfer Equation (29) with respect to $\{n(v,t)\}$ to the moment $\{m_k\}$. The moment transformation involves multiplying Equation (29) by v and then integrating over the entire particle size distribution, and then the governing equation for the k −th moment is expressed as,

$$\frac{\partial m_k}{\partial t}+\frac{\partial(u_j+(u_{th})_j)m_k}{\partial x_j}$$
$$=\frac{\partial}{\partial x_j}\left(\Gamma\frac{\partial m_k}{\partial x_j}\right)+kB_1\hbar m_{k-\frac{1}{3}}\frac{1}{\alpha}+J(v^*)v^{*\,k}$$
$$+\left[\frac{\partial m_k}{\partial t}\right]_{\text{coag}}(k=0,1,2) \qquad (30)$$

where $\left[\frac{\partial m_k}{\partial t}\right]_{\text{coag}}$ is calculated using the Equation (20) of TEMOM-log MOM (I) model. For the unresolved moment, $m_{k-1/3}$ in Equation (30), the closure model in Equation (19) needs to be used to achieve the final closure of equations. In the implementation of TEMOM-log MOM (I) model, only the first three order moments need to be explicitly solved.

Many studies have indicated that sulfuric acid tends to gather water molecules around to form hydrates. These hydrates are considered to stabilize the vapor and reduce the nucleation rate by a factor 10^3~10^8 (Vehkamaki et al., 2003). In the

present study, the advanced parameterization model of Vehkamaki et al. (2003) accounting for high-temperature emissions is used, which is verified to be suitable for the study of particulate matters emitted from engine (Yu et al., 2009). In this new model, the key variables such as nucleation rate $J(v^*)$, the mole fraction and the total number of molecules of sulfuric acid in a critical cluster are taken as functions of temperature, relative humidity and total gas-phase concentration of sulfuric acid.

In the model of Vehkamaki et al. (2003), the mole fraction of sulfuric acid x^* in a critical cluster is given by

$$\begin{aligned} x^* = {} & 0.847012 - 0.0029656T - 0.00662266\ln(Na) + 0.0000587835T\ln(Na) \\ & + 0.0592653\ln(RH) - 0.000363192T\ln(RH) + 0.0230074(\ln(RH))^2 \\ & + 0.0000851374T(\ln(RH))^2 + 0.00217417(\ln(RH))^2 \\ & - 7.923\times10^{-6}T(\ln(RH))^3 \end{aligned} \tag{31}$$

where Na is the total gas-phase concentration of sulfuric acid, T is the absolute temperature and RH is the relative humidity in percentage. The nucleation rate is given by an exponential of a third-order polynomial of $\ln(RH)$ and $\ln(Na)$

$$\begin{aligned} J(v^*) = \exp[& a(T,x^*) + b(T,x^*)\ln(RH) + c(T,x^*)(\ln(RH))^2 + d(T,x^*)(\ln(RH))^3 \\ & + e(T,x^*)\ln(Na) + f(T,x^*)\ln(RH)\ln(Na) + g(T,x^*)(\ln(RH))^2\ln(Na) \\ & + h(T,x^*)(\ln(Na))^2 + i(T,x^*)\ln(RH)(\ln(Na))^2 + j(T,x^*)(\ln(Na))^3 \end{aligned} \tag{32}$$

where the coefficients $a(T,x^*)$ … $j(T,x^*)$ are functions of temperature T and critical cluster mole fraction x^*. The total number of molecules in the critical cluster $\mathrm{N}_{\mathrm{tot}}^*$ is given by

$$\begin{aligned} N_{\mathrm{tot}}^* = \exp[& A(T,x^*) + B(T,x^*)\ln(RH) + C(T,x^*)(\ln(RH))^2 + D(T,x^*)(\ln(RH))^3 \\ & + E(T,x^*)\ln(Na) + F(T,x^*)\ln(RH)\ln(Na) + G(T,x^*)(\ln(RH))^2\ln(Na) \\ & + H(T,x^*)(\ln(Na))^2 + I(T,x^*)\ln(RH)(\ln(Na))^2 + J(T,x^*)(\ln(Na))^3 \end{aligned} \tag{33}$$

where the coefficients $A(T,x^*)$… $J(T,x^*)$ are also functions of temperature T and critical cluster mole fraction x^*. The detailed definitions for these coefficients can be found in the study of Vehkamaki et al. (2003).

In addition, several key functions or parameters, including the velocity of thermophoresis, u_{th}, subgrid-scale turbulent diffusivity coefficient, Γ_{t}, and Brownian diffusion coefficient, Γ_{b}, the growth rate of particle size due to the arrival and loss of the sulfuric acid (H_2SO_4) molecules to the entire droplet surface, G, can be found in (Liu et al., 2019).

4.3.1.3 Governing equations for gas species

During the numerical simulation, the evolution of gas species including sulfuric acid and water vapors, must be determined before making the calculation of moment ODEs. Based on the moment transformation in Equation (4), the differential

equations for the evolution of gas species, including sulfuric acid, Y_1, water vapors, Y_2, and CO_2 tracer, Y_3 are expressed as:

$$\frac{\partial Y_1}{\partial t}+\frac{\partial u_j Y_1}{\partial x_j}=\frac{\partial}{\partial x_j}\left(D_1\frac{\partial Y_1}{\partial x_j}\right)+R-J(v^*)k^*-\frac{B_1}{v^*}\hbar m_{2/3} \qquad (34(a))$$

$$\frac{\partial Y_2}{\partial t}+\frac{\partial u_j Y_2}{\partial x_j}=\frac{\partial}{\partial x_j}\left(D_2\frac{\partial Y_2}{\partial x_j}\right) \qquad (34(b))$$

$$\frac{\partial Y_3}{\partial t}+\frac{\partial u_j Y_3}{\partial x_j}=\frac{\partial}{\partial x_j}\left(D_3\frac{\partial Y_3}{\partial x_j}\right) \qquad (34(c))$$

where $k^*$is the number of sulfuric acid molecules in the critical cluster which is denoted by $k^*=\mathrm{N}_{\mathrm{tot}}^*\cdot x^*$, and R is the birth rate. D_1, D_2 and D_3 are molecular diffusion coefficients of sulfuric acid, water vapors and CO_2 tracer respectively. $k^*$is obtained from the nucleation model of Vehkamaki et al. (2003).

4.3.1.4 Configuration of the computational domain

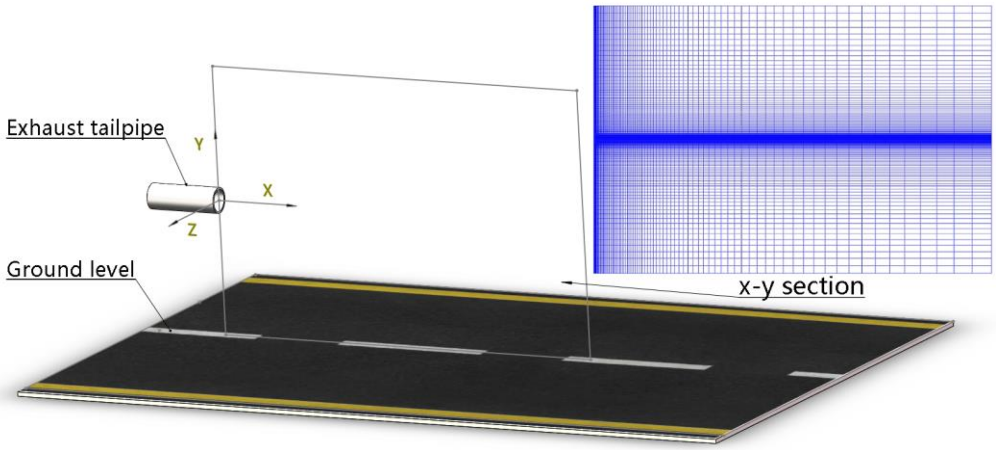

Figure 5 Cartesian coordinate system (*x*, *y*, *z*) of the computational domain

Fig.5 is the Cartesian coordinate system (*x*, *y*, *z*) used in the numerical simulations for the vehicle exhaust plume, which is consistent with the experimental setup shown in (Ning et al., 2005b) and the same as the numerical calculation shown in Yu et al. (2009). The diameter of the vehicle tailpipe is D = 0.03 m. The computational domain is $1000D$ in *x*-coordinate × $333D$ in *y*-coordinate. In order to make comparison with the experimental data and the previous numerical calculation data using the TEMOM model, the tailpipe exit velocity used is 4.8 m/s and the exhaust temperature used is 400 K; H_2O and CO_2 are accounted for 6% and 12% in mole fraction, respectively. The velocity of surrounding air is taken as 0 m/s for the present numerical simulation. The numerical calculation is simplified to be a two-dimensional axisymmetric model which the vehicle tailpipe is a circular pipe.

All the governing equations are discretized by the finite-volume method. The Quadratic Upwind Interpolation for Convective Kinematics (QUICK) scheme is adopted for the convective terms in Equations (28), (30) and (34). For the governing equations accounting for particles and gas species in Equations (30) and (34), a user-defined functions (UDF) in ANSYS Fluent are utilized. The TEMOM-log MOM (I) in Equation (20) is utilized to calculate the evolution of nanoparticle dynamics due to Brownian coagulation. The calculation time step t is fixed to be 0.001 s for all the numerical simulations regarding both the numerical efficiency and accuracy. In the numerical simulation, all calculations are implemented using normalized parameters; the details for the normalization are the same as in our previous research works (Liu**,** et al. Liu, 2019; Yu et al., 2009).

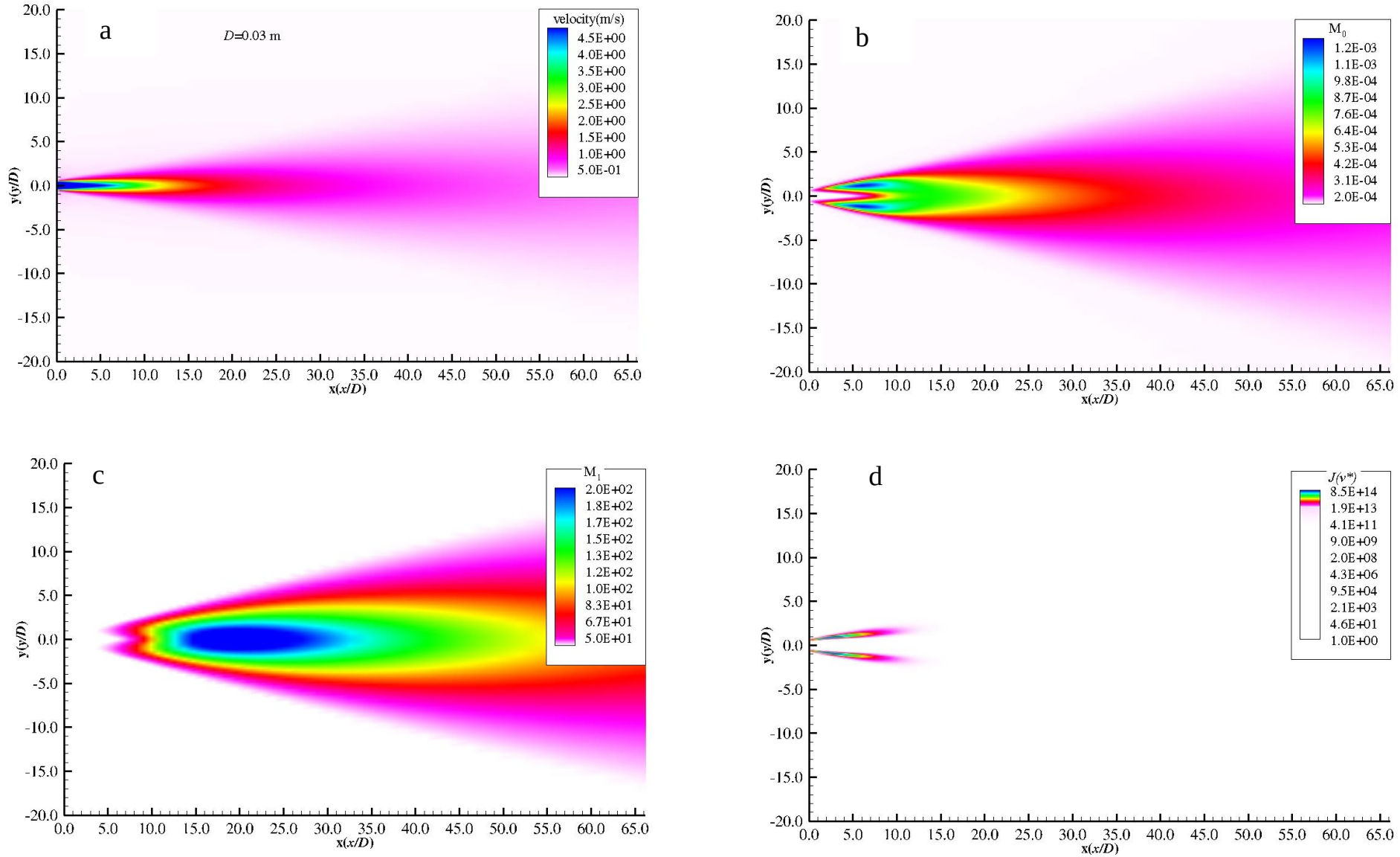

584

585 **Figure 6 The contours of (a) the velocity magnitude (m/s)), (b) the normalized secondary particle number concentration, M_0, (c)**
586 **normalized particle volume concentration, M_1 and (d) nucleation rate of secondary particles, $J(v^*)$ (#/(s· m^3).**

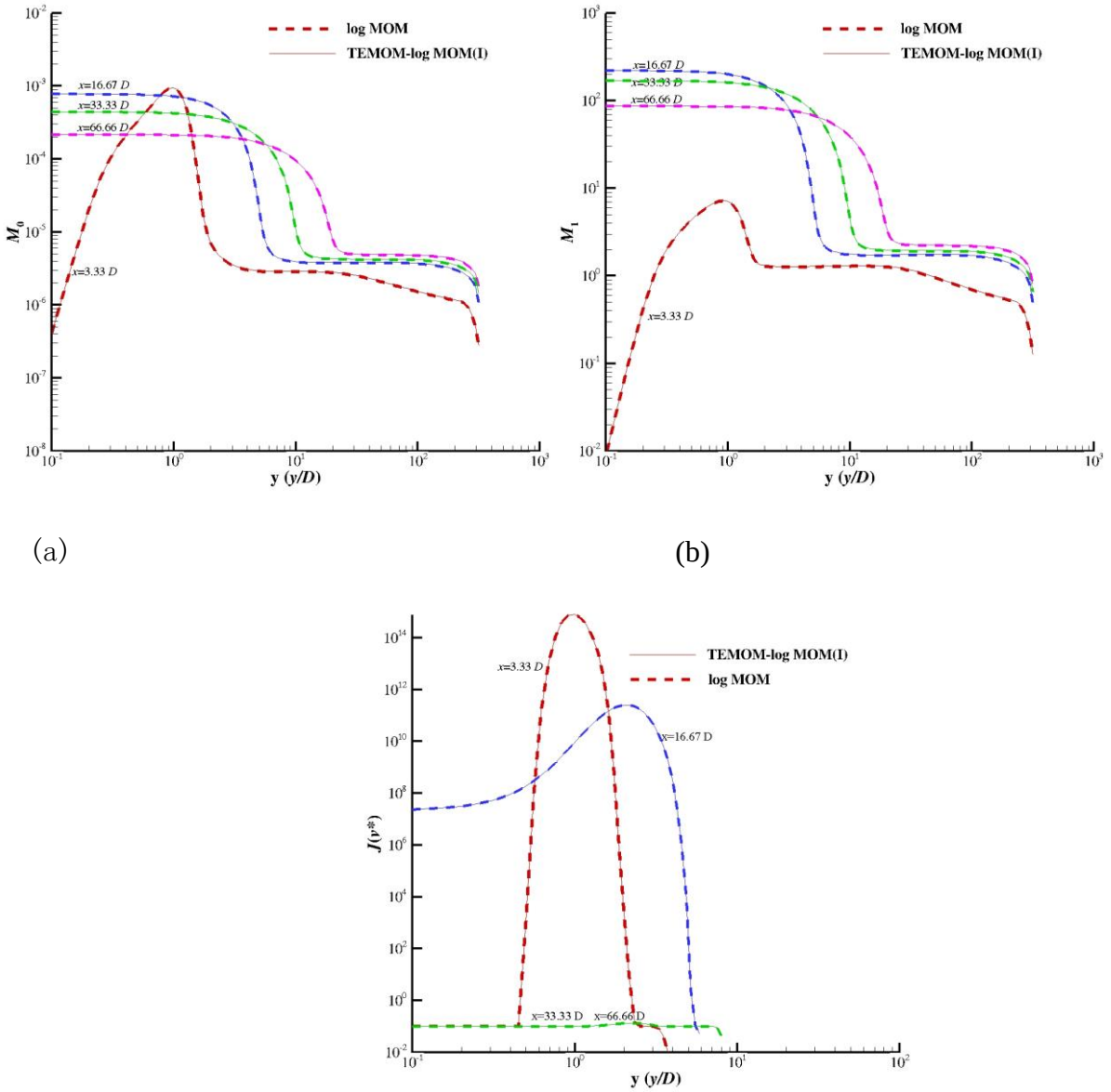

Figure 7 The radial distance, *y* (m) of (a) the normalized secondary particle number concentration, M_0, (b) normalized particle volume concentration, M_1 and (c) nucleation rate of secondary particles at the axial tailpipe exit, *x/D* = 3.33, 16.67, 33.33 and 66.66. Red dot line = 3.33, Pink dot line =16.67, Green dot line = 33.33 and blue dot line = 66.66 in Figures 6(a), (b) &(c).

Figure 6 shows the distribution of (a) the velocity magnitude, (b) normalized secondary particle number concentration, (c) normalized particle volume concentration and (d) nucleation rate of secondary particles. It should be noted both M_0 and M_1 shown in Figures 6(b) and (c) are normalized values according to the normalized equation presented in Eq. (23). In the turbulent jet flow, the evolution of large vortex is found to dominate the distribution and evolution of particle quantities, including the particle number concentration, particle volume concentration, averaged particle size and geometric standard deviation of particle number distribution in the surrounding air condition (Garrick & Khakpour, 2004; Lin et al., 2016).

The effect of the large vortex on the distribution of statistical moment quantities are represented in Figures 6(b) and (c), where the maximum value of particle number concentration appears at the near tailpipe exit $x \approx 0.25{\sim}0.35$ m due to the strong mixture between the exhaust jet flow and the surrounding cold air occurs. In the jet region, the exhaust jet plume temperature decreases to a lower level due to the mixing with the surrounding cold air, and makes the occurrence of binary homogeneous nucleation. It also leads to the high nucleation rate for H_2SO_4-H_2O monomers occurs there, so as the high concentration for the particle number concentration as shown in Figure 6(b). However, it is not surprisingly observed that the main nucleation rate appears only at near tailpipe exit region as shown in Figure 6(d) especially the region is much closer to the tailpipe exit than the high particle number concentration region as shown in Figure 6(b). Further exhaust jet flow downstream, eddies form and entrain the surrounding cold air into the main exhaust jet flow and decrease the gas temperature in the mixing region but no high particle number concentration is formed.

In Figure 6(c), it can be observed that the particle mass concentration reaches the maximum value away from the tailpipe exit at $x \approx 0.50{\sim}0.70$ m. Contrary to the particle number distribution and nucleation rate, the particle mass distribution mainly distributes in the centerline of exhaust jet flow rather in the jet interface. The evolution and distribution of particle dynamics obtained in this study is consistent with the results obtained from the transient method, such as large eddy simulation (Yu et al., 2009), which is the result of external effect such as convection, diffusion and thermophoresis, and the internal dynamic processes (i.e., nucleation, condensation and coagulation). In research group of Garrick (Garrick, 2011; Miller & Garrick, 2004; Murfield & Garrick, 2013) on nanoparticle-laden jet and boundary flows, the new formation of particles on the turbulent interface in boundary layers is also observed, which is considered to be the main source of particle formation in a turbulent flow.

The radial distance of normalized M_0 and M_1, and nucleation rate at different axial exhaust jet distances from the tailpipe exit are shown in Figure 7. Both the newly proposed TEMOM-log MOM (I) model and the widely recognized log MOM model are implemented for the comparative study. There are no obvious difference in the investigated three physical quantities for both MOMs. It should be noted the log MOM is still now the most widely used method in the atmospheric aerosol dynamics due to its high numerical efficiency, for example WRF-Chem in the field of earth science. In Figures 7(a) and (b), it is clear in the region very close to the tailpipe exit, i.e. $x = 0.1$ m, the values of both M_0 and M_1 reach their maximum at the region away from the centerline of the exhaust jet flow, while further exhaust jet flow downstream, $x = 0.5$ to 2.0 m, the values of both M_0 and M_1 in the centerline region of exhaust jet flow are

larger than that in the surrounding region. It implies that in the downstream region, the surrounding air is entrained by large vortices into the nanoparticle-laden multiphase system, which dominates the evolution of the particle dynamics rather than the nucleation process. In Figure 7(c), the nucleation process only appears at $x = 0.1$ and 0.2 m, while further exhaust jet flow downstream at $x = 1.0$ m and 2.0 m, no new particle formation takes place. This is further verified the conclusion from Figure 6(d) that in only the region which new particle can be formed at very near region to the tailpipe exit. In addition, it is clear that the nearer to the tailpipe exit, the higher nucleation rate is formed. The finding would be contrary to the common knowledge that new particles are mostly formed in the region where the jet and the surrounding cold air can be strongly mixed in the downstream exhaust jet flow region (Lin et al., 2016). In the present study, only new particle formation is observed in the jet flow boundary which is very close to the tailpipe exit, while in the downstream exhaust jet flow region where the strong mixture is achieved but no new particle formation is observed. This should contribute to the fact that the number concentration formed of new particles by the main precursor (i.e., H_2SO_4 vapor) cannot meet the minimum requirement to achieve thermally stable H_2SO_4- H_2O monomer in the exhaust jet flow downstream.

5 Conclusions

In the present study, a new mathematical method for solving the SCE undergoing Brownian coagulation in the free molecular regime is firstly proposed and developed. In this method, the concept of well-established TEMOM and log MOM for approximating collision kernel and implicit moments are hybridized. The numerical precision and efficiency of the new method are evaluated by comparing to the SM as well as the TEMOM and classic log MOM. The results imply that the new method in which the collision kernel is approximated with the concept of log MOM and the implicit moments are closed by the concept of TEMOM which has nearly the same numerical precision and efficiency as the TEMOM and log MOM. This new method is further successfully applied to the study of secondary nanoparticle formation and subsequent growth of H_2SO_4-H_2O in a turbulent jet plume. With the new method, the formation of new particles only appears in the interface region of the turbulent exhaust jet which is very close to the tailpipe exit, while there is no new particle formation in the strong mixture between the exhaust jet plume and the surrounding cold air along the downstream. The new method overcomes the limitation of the classical log MOM that the particle size distribution must follow log-normal particle size distributions with respect to time. Thus this new method provides wide applications where the atmospheric aerosol size distribution is typical bimodal or multi-modal cases.

6 Acknowledgments

The authors thank the Zhejiang Provincial Natural Science Foundation of China (LQ16A020002) and the National Natural Science Foundation of China (11872353) for their support. In addition, the original files for Figures 2 to 4 and C programs for the hybrid TEMOM-log MOM method have been archived in the Mendeley data with a name “A hybrid TEMOM-log MOM Method”.

7 Appendix

7.1 The derivation of Equation (11)

$$\beta(v,v_1) = K(1/v + 1/v_1)^{\frac{1}{2}}(v^{\frac{1}{3}} + {v_1}^{\frac{1}{3}})^2$$

$$= K(v+v_1)^{\frac{1}{2}}(v^{\frac{1}{6}}{v_1}^{-\frac{1}{2}} + 2v^{-\frac{1}{6}}{v_1}^{-\frac{1}{6}} + v^{-\frac{1}{2}}{v_1}^{\frac{1}{6}})$$

$$\approx Kb_k(v^{\frac{1}{2}} + v_1^{\frac{1}{2}})(v^{\frac{1}{6}}{v_1}^{-\frac{1}{2}} + 2v^{-\frac{1}{6}}{v_1}^{-\frac{1}{6}} + v^{-\frac{1}{2}}{v_1}^{\frac{1}{6}})$$

$$= Kb_k(v^{\frac{2}{3}}{v_1}^{-\frac{1}{2}} + 2v^{\frac{1}{3}}{v_1}^{-\frac{1}{6}} + v_1^{\frac{1}{6}} + v^{\frac{1}{6}} + 2v^{-\frac{1}{6}}v_1^{\frac{1}{3}} + v^{-\frac{1}{2}}v_1^{\frac{2}{3}})$$

$$\triangleq \tilde{\beta}_{\text{Log}}(v,v_1) \tag{A1}$$

7.2 The derivation of Equation (16)

$$\beta(v,v_1)$$

$$= K(1/v + 1/v_1)^{\frac{1}{2}}(v^{\frac{1}{3}} + {v_1}^{\frac{1}{3}})^2$$

$$= K(v+v_1)^{1/2}(v^{1/6}{v_1}^{-1/2} + 2v^{-1/6}{v_1}^{-1/6} + v^{-1/2}{v_1}^{1/6})$$

$$\approx K(\frac{3\sqrt{2u}}{8} + \frac{3\sqrt{2}v}{8\sqrt{u}} + \frac{3\sqrt{2}v_1}{8\sqrt{u}} - \frac{\sqrt{2}v^2}{32u^{\frac{3}{2}}} - \frac{\sqrt{2}vv_1}{16u^{\frac{3}{2}}} - \frac{\sqrt{2}v_1^2}{32u^{\frac{3}{2}}})(v^{\frac{1}{6}}{v_1}^{-\frac{1}{2}} + 2v^{-\frac{1}{6}}{v_1}^{-\frac{1}{6}} + v^{-\frac{1}{2}}{v_1}^{\frac{1}{6}})$$

$$= K\left[\frac{3}{8}(2u)^{\frac{1}{2}}(2v^{\frac{1}{6}}{v_1}^{-\frac{1}{2}} + 2v^{-\frac{1}{6}}{v_1}^{-\frac{1}{6}}) + \frac{3}{8}(\frac{2}{u})^{\frac{1}{2}}(2v^{\frac{7}{6}}{v_1}^{-\frac{1}{2}} + 4v^{\frac{5}{6}}{v_1}^{-\frac{1}{6}} + 2v^{\frac{1}{2}}v_1^{\frac{1}{6}})\right.$$
$$\left. - \frac{1}{32}(\frac{2}{u^3})^{\frac{1}{2}}(4v^{\frac{5}{6}}v_1^{\frac{5}{6}} + 4v^{\frac{7}{6}}v_1^{\frac{1}{2}} + 2v^{\frac{3}{2}}v_1^{\frac{1}{6}} + 2v^{\frac{13}{6}}{v_1}^{-\frac{1}{2}} + 4v^{\frac{11}{6}}{v_1}^{-\frac{1}{6}})\right]$$

$$\triangleq \tilde{\beta}_{\text{Taylor}}(v,v_1) \tag{A2}$$

7.3 The derivation of Equation (23)

The *k*-th moment with closure function by assuming the log-normal particle size distribution takes the following expression

$$m_k = \int_0^\infty e^{ky} \cdot \frac{N_0}{3\sqrt{2\pi}\ln\sigma} e^{-\frac{(y-\ln v_g)^2}{18\ln^2\sigma}} \mathrm{d}y$$

$$= \frac{N_0}{3\sqrt{2\pi}\ln\sigma} \int_0^\infty e^{-\frac{y^2 - 2(\ln v_g + 9k\ln^2\sigma)y + \ln^2 v_g}{18\ln^2\sigma}} \mathrm{d}y$$

$$= e^{k\ln v_g+\frac{9}{2}k^2\ln^2\sigma}\cdot\frac{N_0}{3\sqrt{2\pi}\ln\sigma}\int_0^{\infty} e^{-\frac{\left(y-\ln v_g-9k\ln^2\sigma\right)^2}{18\ln^2\sigma}}\,\mathrm{d}y$$

$$= m_0 e^{k\ln(v_g)+\frac{9}{2}k^2\ln^2\sigma} \tag{A3}$$

where $N_0(=m_0)$ is the initial total number of particles, v_g is the geometric mean volume. Equation (A3) can be further expressed in terms of m_0, m_1 and m_2:

$$m_k = m_0^{1-\frac{3}{2}k+\frac{1}{2}k^2} m_1^{2k-k^2} m_2^{-\frac{1}{2}k+\frac{1}{2}k^2}.$$

7.4 Normalized moment ODEs

When the Equation (25) is introduced into Equations (20) and (22), the normalized equations for the hybrid models (I) and (II) are obtained as, respectively,

$$\begin{cases} \dfrac{\mathrm{d}M_0}{\mathrm{d}\tau} = -\dfrac{\sqrt{2}M_0^{\frac{59}{36}}}{32M_1^{\frac{29}{9}}M_2^{\frac{7}{36}}}\left(\begin{array}{c} -M_0^{\frac{11}{6}}M_1^{\frac{1}{9}}M_2^{\frac{11}{6}}+12M_0^{\frac{2}{3}}M_1^{\frac{22}{9}}M_2^{\frac{2}{3}}+11M_0^{\frac{1}{2}}M_1^{\frac{25}{9}}M_2^{\frac{1}{2}}+12M_0^{\frac{7}{18}}M_1^{3}M_2^{\frac{7}{18}} \\ +24M_0^{\frac{2}{9}}M_1^{\frac{10}{3}}M_2^{\frac{2}{9}}-2M_0^{\frac{1}{6}}M_1^{\frac{31}{9}}M_2^{\frac{1}{6}}-2M_0^{\frac{19}{18}}M_1^{\frac{5}{3}}M_2^{\frac{19}{18}}-2M_0^{\frac{1}{18}}M_1^{\frac{11}{3}}M_2^{\frac{1}{18}}+12M_1^{\frac{34}{9}} \end{array}\right) \\ \dfrac{\mathrm{d}M_1}{\mathrm{d}\tau} = 0 \\ \dfrac{\mathrm{d}M_2}{\mathrm{d}\tau} = -\dfrac{\sqrt{2}M_0^{-\frac{25}{36}}}{16M_1^{\frac{41}{9}}M_2^{\frac{5}{36}}}\left(\begin{array}{c} M_0^{\frac{23}{6}}M_1^{\frac{1}{9}}M_2^{\frac{31}{9}}-24M_0^{\frac{11}{9}}M_1^{\frac{16}{3}}M_2^{\frac{5}{6}}-12M_0^{\frac{5}{3}}M_1^{\frac{40}{9}}M_2^{\frac{23}{18}}+2M_0^{\frac{13}{6}}M_1^{\frac{31}{9}}M_2^{\frac{16}{9}}+2M_0^{\frac{55}{18}}M_1^{\frac{5}{3}}M_2^{\frac{8}{3}} \\ +2M_0^{\frac{37}{18}}M_1^{\frac{11}{3}}M_2^{\frac{5}{3}}+M_0^{\frac{5}{2}}M_1^{\frac{25}{9}}M_2^{\frac{19}{9}}-12M_0^{\frac{1}{2}}M_1^{\frac{61}{9}}M_2^{\frac{1}{9}}-12M_0M_1^{\frac{52}{9}}M_2^{\frac{11}{18}}-12M_0^{\frac{7}{18}}M_1^{7} \end{array}\right) \end{cases} \tag{A4}$$

and

$$\begin{cases} \dfrac{\mathrm{d}M_0}{\mathrm{d}\tau} = b\dfrac{M_0^{11/6}(41M_0^2M_2^2-190M_0M_1^2M_2-2443M_1^4)}{648M_1^{23/6}} \\ \dfrac{\mathrm{d}M_1}{\mathrm{d}\tau} = 0 \\ \dfrac{\mathrm{d}M_2}{\mathrm{d}\tau} = -b\dfrac{65M_0^2M_2^2-670M_0M_1^2M_2-1987M_1^4}{324M_0^{1/6}M_2^{11/6}}. \end{cases} \tag{A5}$$

References

Ackermann, I. J., Hass, H., Memmesheimer, M., Ebel, a., Binkowski, F. S., & Shankar, U. (1998). Modal aerosol dynamics model for Europedevelopment and first applications. *Atmospheric Environment*, *32*(17), 2981–2999. https://doi.org/10.1016/S1352-2310(98)00006-5

Barrett, J. C., & Jheeta, J. S. (1996). Improving the accuracy of the moments method for solving the aerosol General Dynamic Equation. *Journal of Aerosol Science*, *27*(8), 1135–1142. https://doi.org/10.1016/0021-8502(96)00059-6

Bruns, M. C., & Ezekoye, O. a. (2012). Development of a hybrid sectional quadrature-based moment method for solving population balance equations. *Journal of Aerosol Science*, *54*, 88–102. https://doi.org/10.1016/j.jaerosci.2012.07.003

Cai, C., Zhang, X., Wang, K., Zhang, Y., Wang, L., Zhang, Q., et al. (2016). Incorporation of new particle formation and early growth treatments into WRF/Chem: Model improvement, evaluation, and impacts of anthropogenic aerosols over East Asia. *Atmospheric Environment*, *124*(August 2016), 262–284. https://doi.org/10.1016/j.atmosenv.2015.05.046

Chan, T. L., & Ning, Z. (2005). On-road remote sensing of diesel vehicle emissions measurement and emission factors estimation in Hong Kong. *Atmospheric Environment*, *39*(36), 6843–6856. https://doi.org/10.1016/j.atmosenv.2005.07.048

Chan, T. L., Liu, Y. H., & Chan, C. K. (2010a). Direct quadrature method of moments for the exhaust particle formation and evolution in the wake of the studied ground vehicle. *Journal of Aerosol Science*, *41*(6), 553–568. https://doi.org/10.1016/j.jaerosci.2010.03.005

Chan, T. L., Zhou, K., Lin, J. Z., & Liu, C. H. (2010b). Vehicular exhaust gas-to-nanoparticle conversion and concentration distribution in the vehicle wake region. *International Journal of Nonlinear Sciences and Numerical Simulation*, *11*(8), 581–593. https://doi.org/10.1515/ijnsns.2010.11.8.581

Cohen, E. R., & Vaughan, E. U. (1971). Approximate solution of the equations for aerosol agglomeration. *Journal of Colloid And Interface Science*, *35*(4), 612–623. https://doi.org/10.1016/0021-9797(71)90219-0

Debry, E., Sportisse, B., & Jourdain, B. (2003). A stochastic approach for the numerical simulation of the general dynamics equation for aerosols. *Journal of Computational Physics*, *184*(2), 649–669. https://doi.org/10.1016/S0021-9991(02)00041-4

Fox, R. O., Laurent, F., & Massot, M. (2008). Numerical simulation of spray coalescence in an Eulerian framework: Direct quadrature method of moments and multi-fluid method. *Journal of Computational Physics*, *227*(6), 3058–3088. https://doi.org/10.1016/j.jcp.2007.10.028

Friedlander, S. K. (2000). *Smoke, dust and haze: Fundamentals of aerosol behavior*. (G. L. Rogers, Ed.), *New York Wiley Interscience* (2nd ed.). John Wiley & Sons, Inc. Retrieved from http://adsabs.harvard.edu/abs/1977wi...book.....F

Gama, C., Ribeiro, I., Lange, A. C., Vogel, A., Ascenso, A., Seixas, V., et al. (2019). Performance assessment of CHIMERE and EURAD-IM' dust modules. *Atmospheric Pollution Research*, *10*(4), 1336–1346. https://doi.org/10.1016/j.apr.2019.03.005

Garrick, S. C. (2011). Effects of turbulent fluctuations on nanoparticle coagulation in shear flows. *Aerosol Science and Technology*, *45*(10), 1272–1285. https://doi.org/10.1080/02786826.2011.589482

Garrick, S. C., & Khakpour, M. (2004). The effects of differential diffusion on nanoparticle coagulation in temporal mixing layers. *Aerosol Science and Technology*, *38*(8), 851–860. https://doi.org/10.1080/027868290503091

Gelbard, F., Tambour, Y., & Seinfeld, J. H. (1980). Sectional representations for simulating aerosol dynamics. *Journal of Colloid and Interface Science*, *76*(2), 541–556.

Gnach, A., Lipinski, T., Bednarkiewicz, A., Rybka, J., & Capobianco, J. A. (2015). Upconverting Nanoparticles : Assessing the Toxicity. *Chemical Society Reviews*, *44*(6), 1561–1584.

Grabowski, W. W., Morrison, H., Shima, S. I., Abade, G. C., Dziekan, P., & Pawlowska, H. (2019). Modeling of cloud microphysics: Can we do better? *Bulletin of the American Meteorological Society*, *100*(4), 655–672. https://doi.org/10.1175/BAMS-D-18-0005.1

Harrison, R. M., Rob Mackenzie, A., Xu, H., Alam, M. S., Nikolova, I., Zhong, J., et al. (2018). Diesel exhaust nanoparticles and their behaviour in the atmosphere. *Proceedings of the Royal Society A: Mathematical, Physical and Engineering Sciences*, *474*(2220). https://doi.org/10.1098/rspa.2018.0492

Hass, H., van Loon, M., Kessler, C., Stern, R., Matthijsen, J., S., et al. (2003). Aerosol modeling: results and intercomparison from European regional-scale modeling systems. A contribution to the EUROTRAC-2 subproject GLOREAM., *2*(JANUARY).

Herranz, L. E., Lebel, L., Mascari, F., & Spengler, C. (2018). Progress in modeling in-containment source term with ASTEC-Na. *Annals of Nuclear Energy*, *112*, 84–93. https://doi.org/10.1016/j.anucene.2017.09.037

Herzog, M., Weisenstein, D. K., & Penner, J. E. (2004). A dynamic aerosol module for global chemical transport models: Model description. *Journal of Geophysical Research Atmospheres*, *109*(18).

https://doi.org/10.1029/2003JD004405

Heylmun, J. C., Kong, B., Passalacqua, A., & Fox, R. O. (2019). A quadrature-based moment method for polydisperse bubbly flows. *Computer Physics Communications*, *244*, 187–204. https://doi.org/10.1016/j.cpc.2019.06.005

Huang, R. J., Zhang, Y., Bozzetti, C., Ho, K. F., Cao, J. J., Han, Y., et al. (2014). High secondary aerosol contribution to particulate pollution during haze events in China. *Nature*, *514*(7521), 218–222. https://doi.org/10.1038/nature13774

Jasor, M. S. G., Polifke, P. W., & Ph, D. (2005). Multi-scale Modelling of the Population Dynamics of Hydrometeors with Methods of Moments.

Karydis, V. A., Tsimpidi, A. P., & Pandis, S. N. (2007). Evaluation of a three-dimensional chemical transport model (PMCAMx) in the eastern United States for all four seasons. *Journal of Geophysical Research Atmospheres*, *112*(14). https://doi.org/10.1029/2006JD007890

Kong, B., & Fox, R. O. (2017). A solution algorithm for fluid–particle flows across all flow regimes. *Journal of Computational Physics*, *344*, 575–594. https://doi.org/10.1016/j.jcp.2017.05.013

Korhonen, H., Lehtinen, K. E. J., & Kulmala, M. (2004). Multicomponent aerosol dynamics model UHMA: model development and validation. *Atmospheric Chemistry and Physics*, *4*, 757–771. https://doi.org/10.5194/acpd-4-471-2004

Kostoglou, M. (2007). Extended cell average technique for the solution of coagulation equation. *Journal of Colloid and Interface Science*, *306*(1), 72–81.

Kraft, M. (2005). Modelling of Particulate Processes. *Kona*, *23*(23), 18–35. https://doi.org/10.1016/j.apsusc.2005.03.071

Kruis, F. E., Wei, J., van der Zwaag, T., & Haep, S. (2012). Computational fluid dynamics based stochastic aerosol modeling: Combination of a cell-based weighted random walk method and a constant-number Monte-Carlo method for aerosol dynamics. *Chemical Engineering Science*, *70*, 109–120. https://doi.org/10.1016/j.ces.2011.10.040

Kukkonen, J., Olsson, T., Schultz, D. M., Baklanov, A., Klein, T., Miranda, A. I., et al. (2012). A review of operational, regional-scale, chemical weather forecasting models in Europe. *Atmospheric Chemistry and Physics*, *12*(1), 1–87. https://doi.org/10.5194/acp-12-1-2012

Kumar, P., Morawska, L., Birmili, W., Paasonen, P., Hu, M., Kulmala, M., et al. (2014). Ultrafine particles in cities. *Environment International*, *66*, 1–10. https://doi.org/10.1016/j.envint.2014.01.013

Landgrebe, J. D., & Pratsinis, S. E. (1990). A discrete-sectional model for particulate production by gas-phase chemical reaction and aerosol coagulation in the free-molecular regime. *Journal of Colloid and Interface Science*, *139*(1), 63–86. https://doi.org/10.1016/0021-9797(90)90445-T

Lauer, a., Hendricks, J., Ackermann, I., Schell, B., Hass, H., & Metzger, S. (2005). Simulating aerosol microphysics with the ECHAM/MADE GCM – Part I: Model description and comparison with observations. *Atmospheric Chemistry and Physics Discussions*, *5*(5), 7965–8026. https://doi.org/10.5194/acpd-5-7965-2005

Lee, K. W., Chen, H., & Gieseke, J. A. (1984). Log-Normally Preserving Size Distribution for Brownian Coagulation in the Free-Molecule Regime. *Aerosol Science and Technology*, *3*(1), 53–62.

Lin, J., Pan, X., Yin, Z., & Ku, X. (2016). Solution of general dynamic equation for nanoparticles in turbulent flow considering fluctuating coagulation. *Applied Mathematics and Mechanics (English Edition)*, *37*(10), 1275–1288. https://doi.org/10.1007/s10483-016-2131-9

Liu, H. M., & Chan, T. L. (2016). A new differentially weighted operator splitting Monte Carlo method for aerosol dynamics. *Proceedings of the 24th International Conference on Modelling, Monitoring and Management of Air Pollution (Air Pollution 2016), June 20-22, 2016, Crete, Greece.*, *207*(WIT Transactions on Ecology and the Environment), 237–248. https://doi.org/10.2495/AIR160221

Liu, S., Chan, T. L., & Liu, H. (2019). Numerical simulation of particle formation and evolution in a vehicle exhaust plume using the bimodal Taylor expansion method of moments. *Particuology*, *43*(August 2018), 46–55. https://doi.org/10.1016/j.partic.2018.02.003

Liu, S., Chan, T. L., Lin, J., & Yu, M. (2019). Numerical study on fractal-like soot aggregate dynamics of turbulent ethylene-oxygen flame. *Fuel*, *256*(March), 115857. https://doi.org/10.1016/j.fuel.2019.115857

Marchisio, D. L., & Fox, R. O. (2005). Solution of population balance equations using the direct quadrature method of moments. *Journal of Aerosol Science*, *36*(1), 43–73. https://doi.org/10.1016/j.jaerosci.2004.07.009

Maurya, R. K., Saxena, M. R., Rai, P., & Bhardwaj, A. (2018). Effect of compression ratio, nozzle opening pressure, engine load, and butanol addition on nanoparticle emissions from a non-road diesel engine. *Environmental Science and Pollution Research*, *25*(15), 14674–14689. https://doi.org/10.1007/s11356-018-1644-8

McGraw, R, Leng, L., Zhu, W., Riemer, N., & West, M. (2008). Aerosol dynamics using the quadrature method of moments: comparing several quadrature schemes with particle-resolved simulation. *Journal of Physics: Conference Series*, *125*, 012020. https://doi.org/10.1088/1742-6596/125/1/012020

McGraw, Robert. (1997a). Description of Aerosol Dynamics by the Quadrature Method of Moments. *Aerosol Science and Technology*, *27*(2), 255–265. https://doi.org/10.1080/02786829708965471

McGraw, Robert. (1997b). Description of Aerosol Dynamics by the Quadrature Method of Moments. *Aerosol Science and Technology*, *27*(2), 255–265. https://doi.org/10.1080/02786829708965471

Menz, W. J., Akroyd, J., & Kraft, M. (2014). Stochastic solution of population balance equations for reactor networks. *Journal of Computational Physics*, *256*, 615–629. https://doi.org/10.1016/j.jcp.2013.09.021

Miller, S. E., & Garrick, S. C. (2004). Nanoparticle Coagulation in A Planar Jet. *Aerosol Science and Technology*, *38*(1), 79–89. https://doi.org/10.1080/02786820490247669

Morgan, N., Wells, C., Goodson, M., Kraft, M., & Wagner, W. (2006). A new numerical approach for the simulation of the growth of inorganic nanoparticles. *Journal of Computational Physics*, *211*(2), 638–658. https://doi.org/10.1016/j.jcp.2005.04.027

Müller, H. (1928). Zur allgemeinen Theorie ser raschen Koagulation. *Fortschrittsberichte {ü}ber Kolloide Und Polymere*, *27*(6), 223–250.

Murfield, N. J., & Garrick, S. C. (2013). Large eddy simulation and direct numerical simulation of homogeneous nucleation in turbulent wakes. *Journal of Aerosol Science*, *60*, 21–33. https://doi.org/10.1016/j.jaerosci.2013.01.009

Nagpure, A. S., Gurjar, B. R., & Kumar, P. (2011). Impact of altitude on emission rates of ozone precursors from gasoline-driven light-duty commercial vehicles. *Atmospheric Environment*, *45*(7), 1413–1417. https://doi.org/10.1016/j.atmosenv.2010.12.026

Ning, Z., Cheung, C. S., Lu, Y., Liu, M. A., & Hung, W. T. (2005a). Experimental and numerical study of the dispersion of motor vehicle pollutants under idle condition. *Atmospheric Environment*, *39*(40), 7880–7893. https://doi.org/10.1016/j.atmosenv.2005.09.020

Ning, Z., Cheung, C. S., Lu, Y., Liu, M. A., & Hung, W. T. (2005b). Experimental and numerical study of the dispersion of motor vehicle pollutants under idle condition. *Atmospheric Environment*, *39*(40), 7880–7893. https://doi.org/10.1016/j.atmosenv.2005.09.020

Olin, M., Alanen, J., Palmroth, M. R. T., Rönkkö, T., & Dal Maso, M. (2019). Inversely modeling homogeneous H2SO4-H2O nucleation rate in exhaust-related conditions. *Atmospheric Chemistry and Physics*, *19*(9), 6367–6388. https://doi.org/10.5194/acp-19-6367-2019

Otto, E., Fissan, H., Park, S., & Lee, K. (1999). log-normal size distribution theory of Brownian aerosol coagulation for the entire particle size range: Part II—analytical solution using Dahneke's coagulation kernel. *Journal of Aerosol Science*, *30*(1), 17–34.

Park, S., Lee, K., Otto, E., & Fissan, H. (1999a). log-normal size distribution theory of Brownian aerosol coagulation for the entire particle size range: Part I—analytical solution using the harmonic mean coagulation. *Journal of Aerosol Science*, *30*(1), 3–16. Retrieved from http://www.sciencedirect.com/science/article/pii/S0021850298000378

Park, S., Lee, K., Otto, E., & Fissan, H. (1999b). log-normal size distribution theory of Brownian aerosol coagulation for the entire particle size range: Part I—analytical solution using the harmonic mean coagulation. *Journal of Aerosol Science*, *30*(1), 3–16.

Passalacqua, A., Laurent, F., Madadi-Kandjani, E., Heylmun, J. C., & Fox, R. O. (2018). An open-source quadrature-based population balance solver for OpenFOAM. *Chemical Engineering Science*, *176*, 306–318. https://doi.org/10.1016/j.ces.2017.10.043

Petitti, M., Vanni, M., Marchisio, D. L., Buffo, A., & Podenzani, F. (2013). Simulation of coalescence, break-up and mass transfer in a gas-liquid stirred tank with CQMOM. *Chemical Engineering Journal*, *228*, 1182–1194. https://doi.org/10.1016/j.cej.2013.05.047

Pratsinis, S. E. (1988). Simultaneous nucleation condensation and coagulation in aerosol reactors. *Journal of Colloid & Interface Science*, *124*(2), 416–427.

Rani, S. L., Dhariwal, R., & Koch, D. L. (2014). A stochastic model for the relative motion of high Stokes number particles in isotropic turbulence. *Journal of Fluid Mechanics*, *756*, 870–902. https://doi.org/10.1017/jfm.2014.461

Rosenfeld, D. (2006). Atmosphere. Aerosols, clouds, and climate. *Science (New York, N.Y.)*, *312*(5778), 1323–4. https://doi.org/10.1126/science.1128972

Rosenfeld, D., Sherwood, S., Wood, R., & Donner, L. (2014). Climate effects of aerosol-cloud interactions. *Science*, *343*(6169), 379–380. https://doi.org/10.1126/science.1247490

Rosenfeld, D., Zhu, Y., Wang, M., Zheng, Y., Goren, T., & Yu, S. (2019). Aerosol-driven droplet concentrations dominate coverage and water of oceanic low-level clouds. *Science*, *363*(6427), eaav0566. https://doi.org/10.1126/science.aav0566

Sabelfeld, K. (1998). Stochastic models for coagulation of aerosol particles in intermittent turbulent flows. *Mathematics and Computers in Simulation*, *47*(2–5), 85–101. https://doi.org/10.1016/S0378-4754(98)00095-0

Sportisse, B. (2007). A review of current issues in air pollution modeling and simulation. *Computational Geosciences*, *11*(2), 159–181. https://doi.org/10.1007/s10596-006-9036-4

Tang, H., & Lin, J. Z. (2013). Modeling of scattering properties of mineral aerosols using modified beta function. *Journal of Geophysical Research Atmospheres*, *118*(11), 5570–5587. https://doi.org/10.1002/jgrd.50343

Vehkamaki, H., Kulmala, M., Lehtinen, K. E. J., & Noppel, M. (2003). Modelling Binary Homogeneous Nucleation of Water-Sulfuric Acid Vapours: Parameterisation for High Temperature Emissions. *Environmental Science and Technology*, *37*(15), 3392–3398.

Vignati, E., Wilson, J., & Stier, P. (2004). M7: An efficient size-resolved aerosol microphysics module for large-scale aerosol transport models. *Journal of Geophysical Research D: Atmospheres*, *109*(22), 1–17. https://doi.org/10.1029/2003JD004485

Vikas, V., Wang, Z. J., & Fox, R. O. (2013). Realizable high-order finite-volume schemes for quadrature-based moment methods applied to diffusion population balance equations. *Journal of Computational Physics*, *249*, 162–179. https://doi.org/10.1016/j.jcp.2013.05.002

Wang, J. S., Chan, T. L., Cheung, C. S., Leung, C. W., & Hung, W. T. (2006). Three-dimensional pollutant concentration dispersion of a vehicular exhaust plume in the real atmosphere. *Atmospheric Environment*, *40*(3), 484–497. https://doi.org/10.1016/j.atmosenv.2005.09.046

Wang, Y., Wang, Y., Wang, L., Petäjä, T., Zha, Q., Gong, C., et al. (2019). Increased inorganic aerosol fraction contributes to air pollution and haze in China. *Atmospheric Chemistry and Physics*, *19*(9), 5881–5888. https://doi.org/10.5194/acp-19-5881-2019

Whitby, E. R., & McMurry, P. H. (1997). Modal Aerosol Dynamics Modeling. *Aerosol Science and Technology*, *27*(6), 673–688. https://doi.org/10.1080/02786829708965504

Wright, D. L., Kasibhatla, P. S., McGraw, R., & Schwartz, S. E. (2001). Description and evaluation of a six-moment aerosol microphysical module for use in atmospheric chemical. *Journal of Geophysical Research*, *106*(D17), 20275–20291.

Yao, L., Garmash, O., Bianchi, F., Zheng, J., Yan, C., Kontkanen, J., et al. (2018). Atmospheric new particle formation from sulfuric acid and amines in a Chinese megacity. *Science*, *361*(6399), 278–281. https://doi.org/10.1126/science.aao4839

Yu, M. Z., & Lin, J. (2017a). Hybrid method of moments with interpolation closure–Taylor-series expansion

method of moments scheme for solving the Smoluchowski coagulation equation. *Applied Mathematical Modeling*, *10.1016/j.* https://doi.org/10.1080/02786826.2017.1319566

Yu, M.Z., & Lin, J. (2017b). New scheme for implementing the method of moments with interpolative closure. *Aerosol Science & Technology*, *51*(8), 956–971.

Yu, M.Z., & Lin, J. (2018). Taylor series expansion scheme applied for solving population balance equation. *Reviews in Chemical Engineering*, *34*(4), 561–594. https://doi.org/10.1515/revce-2016-0061

Yu, M.Z., Lin, J., & Chan, T. (2008). A new moment method for solving the coagulation equation for particles in Brownian motion. *Aerosol Science and Technology*, *42*(9), 705–713.

Yu, M. Z., Liu, Y., Lin, J., & Seipenbusch, M. (2015). Generalized TEMOM Scheme for Solving the Population Balance Equation. *Aerosol Science and Technology*, *49*(11), 1021–1036. https://doi.org/10.1080/02786826.2015.1093598

Yu, M.Z., Liu, Y., Jin, G., & Jin, H. (2016). A new analytical solution for agglomerate growth undergoing Brownian coagulation. *Applied Mathematical Modeling*, *40*, 5497–5509.

Yu, M.Z., Lin, J., & Chan, T. L. (2009). Numerical simulation for nucleated vehicle exhaust particulate matters via the TEMOM/LES method. *Int. J. Mod. Phys. C*, *20*(3), 399–421. Retrieved from http://www.worldscinet.com/abstract?id=pii:S0129183109013753

Yuan, Q., Xu, J., Wang, Y., Zhang, X., Pang, Y., Liu, L., et al. (2019). Mixing State and Fractal Dimension of Soot Particles at a Remote Site in the Southeastern Tibetan Plateau. *Environmental Science & Technology*, *53*(14), 8227–8234. research-article. https://doi.org/10.1021/acs.est.9b01917

Zhou, C., Zhang, X., Gong, S., Wang, Y., & Xue, M. (2016). Improving aerosol interaction with clouds and precipitation in a regional chemical weather modeling system. *Atmospheric Chemistry and Physics*, *16*(1), 145–160. https://doi.org/10.5194/acp-16-145-2016

Zhou, K., & Chan, T. L. (2011). Simulation of homogeneous particle nucleation in a free turbulent jet. *Aerosol Science and Technology*, *45*(8), 973–987. https://doi.org/10.1080/02786826.2011.572935